Master’s thesis

Master of science in environmental and land engineering-Climate change

Wave attenuation properties of eelgrass meadows estimated from dynamically-scaled experiments

Supervisor(s):
Prof. Costantino Manes
Dr. Davide Vettori

Candidate:
Amirarsalan Shahmohammadi
(s289758)

Politecnico di Torino
2023

Declaration

I hereby declare that, the contents and organization of this dissertation constitute my own original work and does not compromise in any way the rights of third parties, including those relating to the security of personal data.

Amirarsalan Shahmohammadi

March, 2023

I would like to dedicate this thesis to my loving Irene and my precious family

Acknowledgement

I would like to acknowledge professor Costantino Manes for trusting and providing me with opportunity to gain a real research experience, and Dr Davide Vettori for his subtle and thoughtful guidance within this journey.

Abstract

Given the global warming, sea level rise and its associated hazards to coastal zones (i.e., erosion) are inevitable. Being more sustainable, Nature-based coastal protections are being promoted and applied more than ever. Underwater vegetation in shallow waters such as eelgrass, as a nature-based mean, is capable of reducing the wave height coming to the shore yet they have not been thoroughly studied and addressed in the literature. This study assesses the eelgrass wave attenuation ability and the associated properties through a set of dynamically scaled simulation experiments on wave-vegetation interaction. The experiments were conducted in the wave flume equipped with a piston wavemaker and resistant wave gauges to record wave heights. A wide range of wave conditions and water levels was taken into account for different vegetation densities aiming to obtain a more robust result. Eventually, a wave dissipation coefficient was estimated for the eelgrass meadows from the experimental data and was compared with the predicting analytical model proposed in the literature. A relatively reasonable agreement was observed between the experimental result and the predicting model which given the tested wide range of wave and water levels proves the accountability of the predicting model.

Contents

List of Figures

List of Tables

Chapter 1

Introduction

1.1 background

Humans and the sea are inseparable key players on planet earth. Seas have been essential to humans by providing them with food and trade opportunities as well as balancing the climate on earth. In human history, communities developed alongside coasts across the globe. Coastal zones are hosting about 38 per cent of the world's population (Barbier, 2015) as well as significant infrastructures. Regarding the population density, coastal zones stand considerably higher than the in-land areas (Balk et al., 2009) and communities are expanding faster in the former than in the latter areas (Hugo, 2011; Seto, Fragkias, Güneralp, & Reilly, 2011). In low-elevation coastal zones (below 10 m of elevation) it is estimated at least 1 billion people to be inhabited by 2060 (Neumann, Vafeidis, Zimmermann, & Nicholls, 2015). In China, as an example, coastal urban areas are developing three times faster than in-land communities (McGranahan, Balk, & Anderson, 2007). Almost 10 per cent of the gross domestic product (GDP) of China comes from the marine trade and approximately 85 per cent of the country's international trade is facilitated through the ports and marine transport (Zhao, Hynes, & Shun He, 2014). Coming to the west of the world, New York City, home of the giant skyscrapers, known as the world's leading financial centre and hosting the United Nations headquarter located on the west coast of the United States. In Europe, 90 per cent of trade with developing countries and 30 per cent of intra-EU's are carried out through the ports (Mangan, Lalwani, & Fynes, 2008).

Coastal zones, however, are at risk due to natural hazards such as erosion, storms, storm surge due to the storm, tsunami, and flooding (Kaiser & Witzki, 2004). Further, the Global Mean Sea level (GMSL) driven by global warming and consequent ice sheet melting has risen from 1.4 mm/yr in 1901-1990 to 2.1 mm/yr, 3.2 mm/yr, and 3.6 mm/yr in 1970-2015, 1993-2015, and 2006-2015 (IPCC, 2022). As a result, there has been an increase in wave power, (Reguero, Losada, & Méndez, 2019) intensity and frequency of flooding and erosion in coastal zones (IPCC, 2022). The projection scenarios (representative concentration pathway) RCP 2.6, RCP 4.5, and

RCP 8.5 indicate an increase of 0.39, 0.49, and 0.71 m/yr in GMSL, respectively in 2081-2100 relative to 1986-2005 (IPCC, 2022). The projections are reproduced on global and regional scales in figures 1.1 and 1.2. respectively. Thus, it is expected that coastal protection strategies take into account the changing climate.

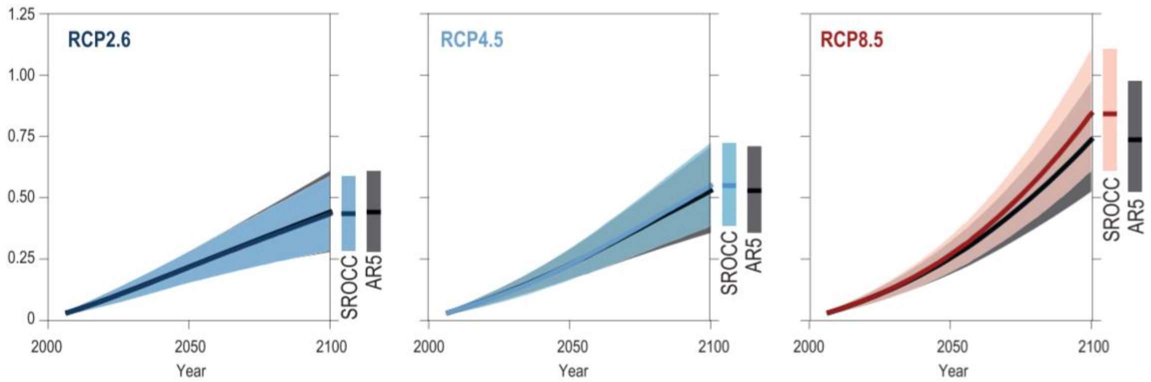

Fig.1.1 Global mean sea level rise (IPCC, 2022)

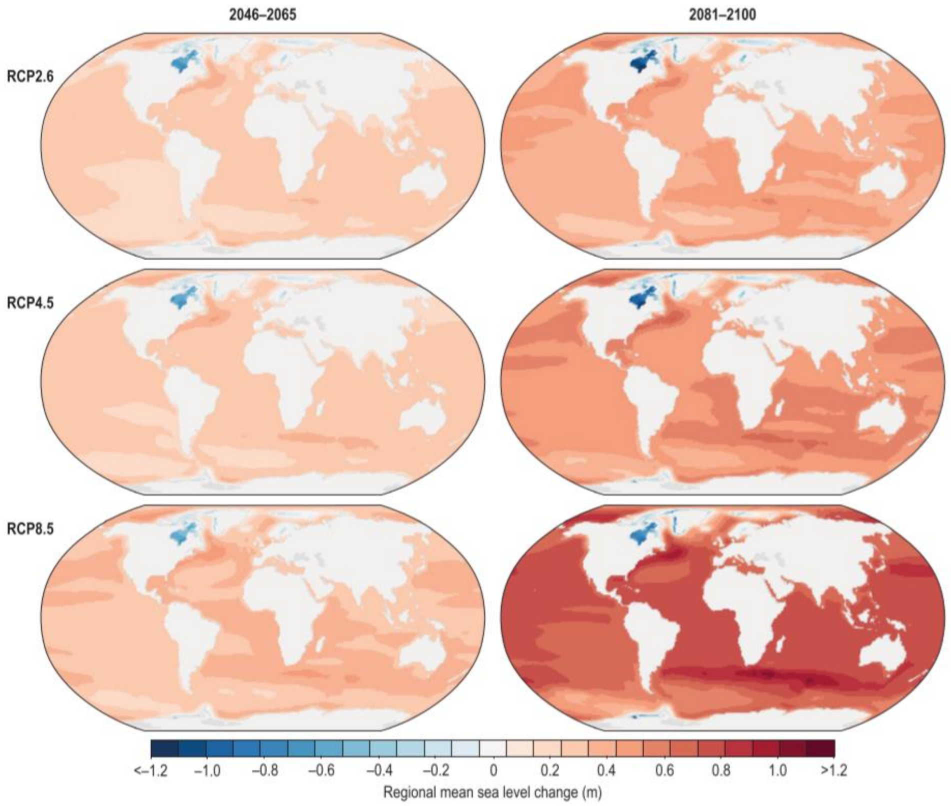

Fig.1.2 Regional mean sea level rise (IPCC, 2022)

1.2 Coastal protection

According to the European Environmental Agency, a set of steps required to preserve the coastline from erosion by of mechanical or vegetational means is defined as coastal protection (EEA Glossary, n.d.). Humans' attempts to defend the coastline go back ages in history ever since they established settlements along the shores. As far as Europe is concerned, it seems the Dutch people were the pioneers, at least in northern Europe, in protecting the coasts by building earth mounds thousand years ago followed by dykes construction in the 11th century (Charlier, Chaineux, & Morcos, 2005). Later seawalls were introduced as a measure inspired by castles and fortes made of clays and stones. Groins or breakwaters were built, more recently, in Britain and Denmark as well as Northern America and kept developing by other European nations i.e. Belgium, the Netherlands, and France.

All the protecting measurements were to dissipate wave energy approaching the shoreline while controlling the sediment transport too in case of breakwaters. Protection systems, nevertheless, can be categorised into different groups parallel to the shoreline, normal to the shoreline, artificial nourishment, and a combination of them. A prudent classification though suggests dividing the coastal defence systems into the "Hard" and "Soft" practices based on their response to the ocean dynamics (Benassai, 2006).

1.2.1 Traditional solutions

Breakwaters, groins, dikes, revetments, and seawalls are major types of hard defensive systems commonly implemented in coastal zones. Breakwaters and groins are adopted in the foreshore prevalently where breakwaters could be submerged or emerged parallel to the shore. Being made of concrete, rocks, sandbags, or geotextiles (Schoonees et al., 2019), breakwaters reflect the wave back to the sea yet transmit some water through their porous structure _ within which some energy is lost due to friction (Pilarczyk, 2003). Groins are usually designed to lay down perpendicular to the shoreline using materials such as rock, timber, or concrete (U S Army Corps Of Engineers, 2002). Besides wave dissipation, groins prevent longshore sediment transport. Both systems though bring about unintentional erosion effects on the downdrift side. Figure 1.3 elaborates Groyne and Breakwater's design and features.

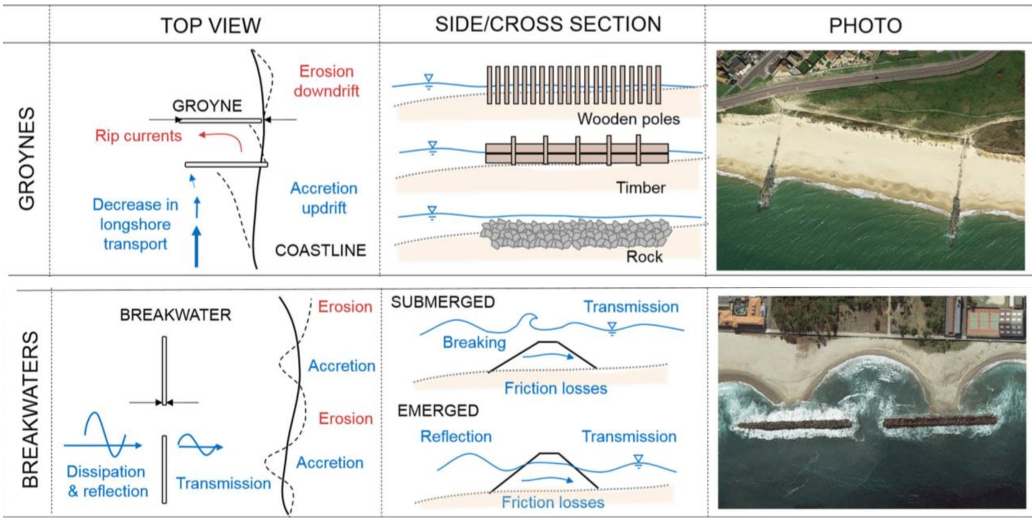

Fig.1.3 Overview of hydrodynamic and morphodynamic effects of groynes and breakwaters (Schoonees et al., 2019)

On the other hand, seawalls, dikes, and revetments are those hard structures designed for onshore areas. Seawalls are reinforced concrete structures constructed along the shore mainly to withstand overtopping and flooding meanwhile maintaining the beach equilibrium. They are, however, associated with the scouring effect at the sea-wall intersection. When erosion is the main concern, revetments might be preferred, being inclined, to blanket the shore dissipating the energy of the incoming waves. Revetments are usually made of rock boulders and cobbles. The scouring effect and inhabiting of non-local species, however, are inevitable impacts interconnected with revetments. With a design parallel to the shore, sea dikes might be used as flood protection in coastal zones made of a sandy core and inclined sides that are covered either by vegetation or rocks considering low and high tide, respectively (Schoonees et al., 2019).

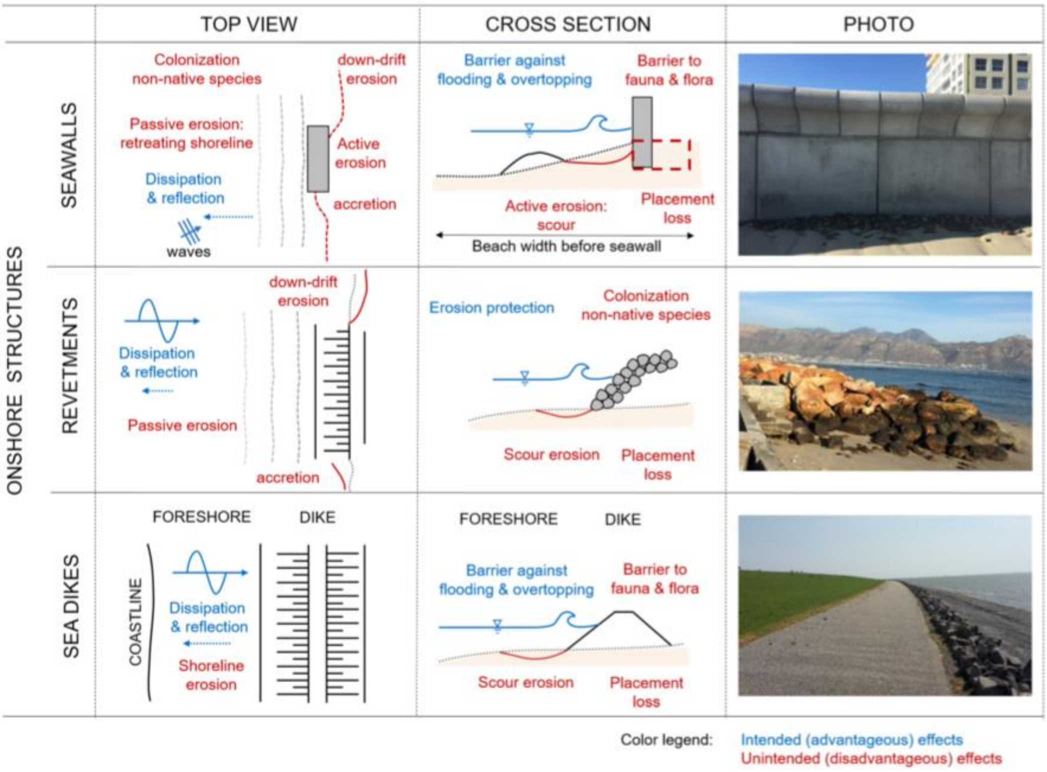

Fig 1.4. Overview of hydrodynamic and morphodynamic effects of seawalls, revetments, and sea dikes (Schoonees et al., 2019)

The set of measures that does not involve structures and in particular massive construction efforts meanwhile providing coastline protection, mainly against erosion, is considered soft coastal protection. Artificial nourishment is the most common method for soft intervention at the shore where the sands extracted either from the sea bottom or land are deposited in the eroded areas along the shore. This practice leads to prompt shore accretion, yet ecological impacts are imminent. Where dunes are shaping the coastline, they can be consolidated and restored using sediments compliant with the area. Dune restoration is environmental-friendly though is limited depending on the width of the beach (Benassai, 2006).

1.2.2 Nature-based solutions (NBS)

Both hard and soft measures could cause coastal ecosystem hazards following by either hydrodynamic or morphologic changes i.e., altering the wave regime, sediment transport and deposition (J. E. Dugan, Airoldi, Chapman, Walker, & Schlacher, 2012). Upon construction of structures such as seawalls and dikes, there is a portion of the beach excavated and lost which results in local habitat loss too (J. E. Dugan et al., 2012; Nordstrom, 2014). This happens too where due to the scouring and erosion at the intersection of the structure and shore bottom, in a long-term period, the shoreline recedes (Griggs & Patsch, 2019) while induced flow at the scouring area may prevent organisms, i.e., sessile, to settle (Gerhart, 1990). Such barriers inhibit species from pursuing inland habitats to breed (Lucrezi, Schlacher, & Robinson, 2010) meanwhile terminating intertidal habitat (J. E. Dugan et al., 2012; Nordstrom, 2014). The induced imbalance in microorganisms' habitat and population within the upper intertidal zone could affect the shorebirds' life (Jenifer E. Dugan, Hubbard, Rodil, Revell, & Schroeter, 2008). Furthermore, non-local species could colonise in a newly-formed rough habitat owing to protecting structure (Firth et al., 2014). Soft measures also, such as artificial nourishment, can lead to biota burial (Schoonees et al., 2019).

Adopting and promoting solutions, thus, by which the coastal environment and ecosystems would be well-preserved, should be deemed crucial and this happens by taking the advantage of the coast's natural features and is called “Nature-Based Solutions” (NBS). Nevertheless, NBS can be categorized as completely natural (e.g. naturally grown seagrasses, coral reefs, mangroves, and saltmarshes), managed natural (planted saltmarshes, artificial coral reefs), hybrid; natural-structural (e.g. marsh-levee system), and environment-friendly structural (e.g. bamboo sediment fences) (Pontee, Narayan, Beck, & Hosking, 2016). In the context of completely and managed natural NBS, as far as wave attenuation and shoreline stabilization are concerned, saltmarshes, mangroves, coral reefs and seagrasses play pivotal roles (IPCC, 2022). Marsh and mangroves can extract the sediments leading to wetlands growth and accumulation of organic material (Kirwan & Megonigal, 2013). This maintains the ecosystem's health and productiveness where these plants can grow in length so that they can interact with the incoming waves (Kirwan, Temmerman, Skeehan, Guntenspergen, & Fagherazzi, 2016). Coral reefs can diminish wave energy by 97% (Ferrario et al., 2014). They buffer the coastline against incoming waves while breaking and damping them. Nevertheless, Mangroves, saltmarshes, and coral reefs are in grave danger due to climate change impact i.e., ocean warming and acidification, as well as Sea Level Rise (SLR) (IPCC, 2022). Seagrasses, on the other hand, are naturally more tolerant of SLR (IPCC, 2022) and in the case of ocean acidification, they are expected to be more productive due to enhanced photosynthesis (Repolho et al., 2017). Seagrasses are the most abundant underwater ecosystem in Europe where 7 out of 60 different species are found; Halophila decipiens, Cymodocea nodosa, Posidonia oceanica, Zostera marina, Zostera noltii, Ruppia maritima and Halophila stipulacea (Ondiviela et al., 2014). Originated in European temperate waters, Cymodocea nodosa, Posidonia oceanica, Zostera marina, and Zostera noltii are of even greater importance (fig 1.5). Concerning coastal protection benefits, seagrasses substantially abate current velocity as well as wave energy (Ondiviela et al., 2014) which may lead to coast survival on flood and erosion. This occurs when waves propagate over the seagrass meadows and on top of the canopy the orbital velocity is influenced by the drag forces of the seagrasses' blades. In other words, being an oscillatory flow, the water's vertical displacement onto the meadows enhances the orbital velocity passage through the seagrasses' blades resulting in reduced flow velocity and wave height.

Fig 1.5. Detail of morphology of seagrass species (Borum, Duarte, Krause-Jensen, & Greve, 2004)

1.3 Study objectives

The aim of the present study was to characterise the wave attenuation properties of seagrass meadows with a set of experiments performed in a wave flume at the hydraulic labarotory of the Politecnico di Torino. Regular waves were generated by means of a wavemaker with different frequencies and periods in different water depths. A seagrass meadow was designed and modelled based on the morphological and mechanical properties of several seagrass species mimicking the real canopies and were installed in the flume in four different densities during the experiments. Eventually, the wave attenuation due to the eelgrass meadows was evaluated using the water surface measurements in the flume collected by resistance wave gauges and the result was compared to the most recent model available in the literature. At last, the governing factors for the wave attenuation due to the eelgrass meadow were assessed and discussed.

Chapter 2

Literature review

2.1 Background theory

The sea water surface is exposed to the air where a wind gust can exert a force on it leading to water surface fluctuation or “waves”. In fact, the wind is the major source of creating sea water waves. Thereafter, the gravitational and surface tension forces enhance wave propagation by providing restoring forces. Besides water depth, the length and height of the wave are the most important characteristics describing the waves through which, however, kinematic characteristics of the waves, i.e., velocity and acceleration, can be derived (Dean & Dalrymple, 1984). Different wave theories have been developed by scholars which are capable of providing wave characteristics using mathematics given reasonable assumptions relevant to the wave propagation patterns. Real sea waves, either random or irregular being, do not simply follow a sinusoidal (cosinusoidal) wave pattern. Yet in shallow waters, where seagrasses inhibit, they relatively tend to be regular which makes it reasonable to consider a sinusoidal behaviour for them (Dean & Dalrymple, 1984). Such sinusoidal behaviour where waves comprise constant height and length within a constant water depth (regular waves) is well addressed by the “linear wave theory” developed by Airy (Airy, 1845). Figure 3.6 represents the expected regular wave and its characteristics according to the linear wave theory. Regular wave characteristics and properties required for the data analysis in this study are provided in the following.

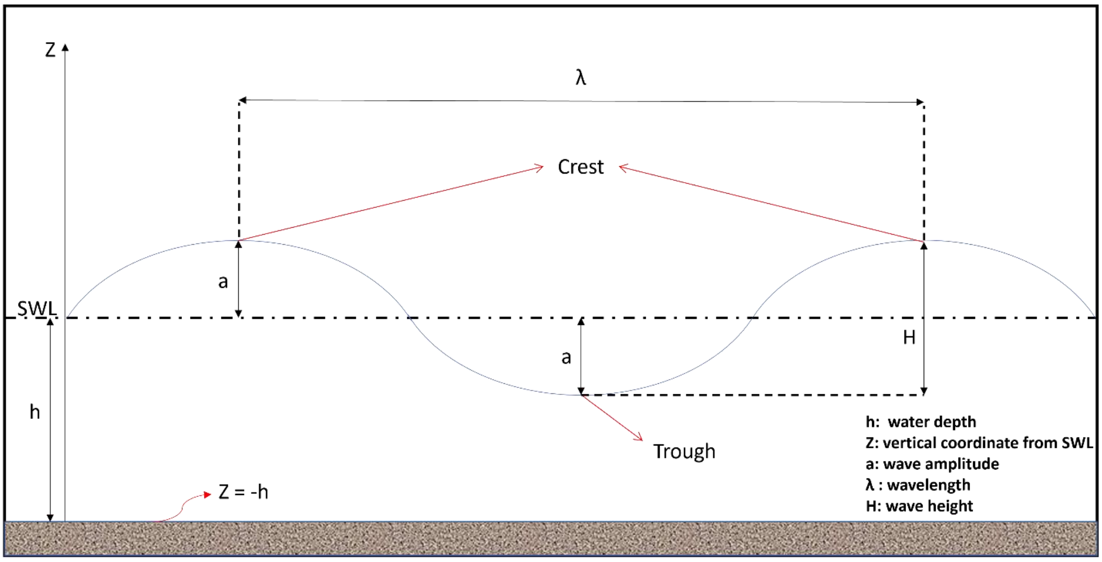

Fig 2.1 Wave characteristics in Linear wave theory

As argued before, each theory bears a set of assumptions to describe the sea waves. As for the linear wave theory it is assumed:

- Constant water density being homogeneous and incompressible the water
- Negligible surface tension
- Negligible earth's Coriolis effect
- Constant and uniform pressure at the surface
- The water is inviscid or ideal
- The flow is irrotational and consequently, water particles do not rotate
- The bottom boundary is fixed, horizontal, and impermeable
- Waves do not change in time and space
- Wave amplitudes are small
- Waves are long-crested (two-dimensional)

Given the irrotational flow, the potential velocity (Φ) concept is permissible whose gradient at any point within the water in either direction, wave propagation x and vertical z, gives the velocity vectors; u and w, respectively (eq.2.1 and 2.2). Being inviscid, the water flow is governed by the Laplace equation (eq. 2.3).

$$u = \frac{\partial \Phi}{\partial x} \tag{2.1}$$

$$w = \frac{\partial \Phi}{\partial z} \tag{2.2}$$

$$\frac{\partial^2 \Phi}{\partial x^2} + \frac{\partial^2 \Phi}{\partial z^2} = 0 \tag{2.3}$$

The fundamental wave characteristics, wavelength (λ), which is related to the wave period (T) as the time required for the water surface to move between two successive peaks, and height (H), are defined as the horizontal distance between crests (troughs) of two successive waves and the vertical distance between the crest and trough within them, respectively (fig 2.1). For the wave height, nevertheless, an average per each experiment is to be calculated (eq.2.4)

$$H = \sqrt{8} \times \sqrt{\frac{\int_0^T \eta^2(t)dt}{T}} \tag{2.4}$$

Where η is the water surface level and T is the wave period.

The water's surface level (η) as a function of time (t) and horizontal distance (x) within a regular wave is expressed as

$$\eta = a\cos(kx - \omega t) = \frac{H}{2}\cos(\frac{2\pi x}{\lambda} - \frac{2\pi t}{T}) \tag{2.5}$$

Where a and ω in turn are the wave amplitude and angular frequency.

The wave phase velocity, also called wave celerity (C), implies how fast an individual waveform propagates and can be obtained using either the ratio between wavelength to the period or the *dispersion* equation (eq 3.6) which varies with water depth (h) and the wave number (k)(eq. 2.7).

$$C = \frac{\lambda}{T} \tag{2.6}$$

$$C = \frac{g\lambda}{2\pi}\tanh(\frac{kh}{2\lambda}) \tag{2.7}$$

Concerning the present study though, the wave orbital velocity and wave group velocity (C_g) are of great interest as they refer to the fluid local velocity (eq.2.1-2.2) i.e., on top of the seagrass canopy and wave train travel speed i.e., velocity per each experiment, respectively. Orbital velocities relationships can be rewritten for both horizontal (u) and vertical (v) velocities as

$$u = \frac{H}{2}\,\omega\,\frac{\cosh k(h+z)}{\sinh kh}\cos(kx - \omega t) \tag{2.8}$$

$$w = \frac{H}{2}\,\omega\,\frac{\sinh k(h+z)}{\sinh kh}\sin(kx - \omega t) \tag{2.9}$$

And the group velocity is expressed using the following relationship.

$$C_g = \frac{1}{2}\frac{\lambda}{T}\left[1 + \frac{\frac{4\pi h}{\lambda}}{\sinh\left(\frac{4\pi h}{\lambda}\right)}\right] \tag{2.10}$$

Last but not least wave characteristic prominent in this study is the water particle displacement which varies from an elliptical to a circular pattern moving from shallow to deep water, respectively (figure 2.2). In other words, water particles move in closed elliptical or circular orbits. Being shallow and intermediate waters of interest in the present study, water particle displacement within an elliptical path is described both horizontally and vertically which is also referred to as wave horizontal/vertical excursion. They can be measured by obtaining ellipse major and minor semi-axis A and B for horizontal and vertical wave excursion, respectively.

$$A = \frac{H}{2}\,\frac{\cosh\left(\frac{2\pi(h+z)}{\lambda}\right)}{\sinh\left(\frac{2\pi h}{\lambda}\right)} \tag{2.11}$$

$$B = \frac{H}{2}\,\frac{\sinh\left(\frac{2\pi(h+z)}{\lambda}\right)}{\sinh\left(\frac{2\pi h}{\lambda}\right)} \tag{2.12}$$

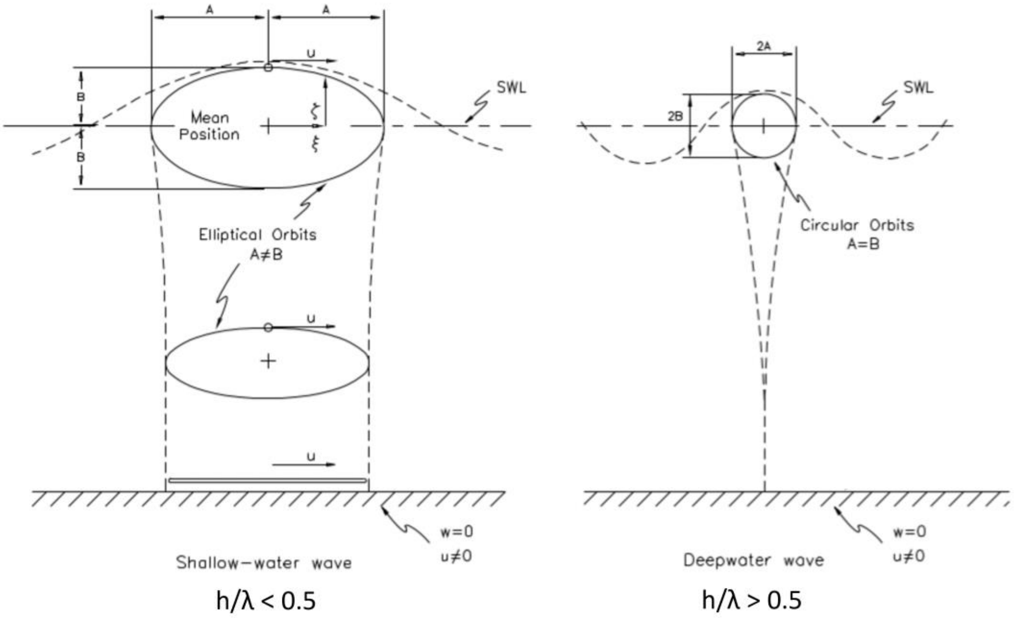

Fig 2.2 Water particle displacement in different water depths (U S Army Corps Of Engineers, 2002)

2.2 State-of-the-art

The wave attenuation studies began with a parabolic model describing regular wave diffraction/refraction including a dissipation coefficient for wave energy introduced in 1984 (Dalrymple, Kirby, & Hwang, 1984). Dalrymple et al. modified a previously introduced parabolic formula (Radder, 1979) for wave propagation such that energy dissipation is also considered. They demonstrated wave height reduction in presence of submerged cylinders/plants (rigid) using the energy conservation concept for a flat seabed condition. Accordingly, a steady energy balance can be expressed using water density (ρ), gravitational acceleration (g), wave amplitude (a), and wave group velocity (C_g) to show the wave energy dissipation rate (E) as follows.

$$-E = \frac{\partial}{\partial x}(\frac{1}{2}\rho g a^2 C_g) \tag{2.13}$$

Being predominantly governed by the drag force, the dissipation rate over the rigid body length (l) reads

$$E = \int_{z=0}^{l} (\frac{1}{2}\rho C_D A u|u|\, dz) \tag{2.14}$$

Where C_D, A, and u are the drag coefficient, rigid body area, and wave horizontal orbital velocity, respectively. It should be noted that z is zero at the bottom of the flume. Eventually, assuming a constant C_g, being constant the water depth, the solution for equation 2.13 is derived (Dalrymple et al., 1984).

$$\frac{a}{a_0} = \frac{1}{1 + K_D x} \tag{2.15}$$

Where a_0 is the incident wave amplitude upon arriving in the meadow and K_D is the dissipation coefficient at distance x from the incident wave and reads

$$K_D = \frac{2C_D}{3\pi}\left(\frac{D}{b}\right)\left(\frac{a_0}{b}\right) sinh^3 kl + 3\sinh kl)\left[\frac{4k}{3\sinh kh(\sinh 2kh + 2kh)}\right] \tag{2.16}$$

Where D and b are the plant diameter and the space between the plants, respectively.

This concept of assuming rigid vegetation was adopted by other scholars for further studies on seagrasses and wave interaction. Laboratory studies on the same topic were done assuming vegetation to be rigid or with a significantly lower velocity than the orbital velocity above the meadow_ quasi-rigid vegetation (Asano, Deguchi, & Kobayashi, 1993; Kobayashi, Raichle, & Asano, 1993; Mendez & Losada, 2004; Méndez, Losada, & Losada, 1999). As for the wave height reduction due to the vegetation, another relationship based on the continuity and momentum equation describing exponential decay assuming a horizontal bed was introduced as follows (Kobayashi et al., 1993).

$$H = H_0 e^{-k_i x} \tag{2.17}$$

Where H, H_0, k_i, and x are the local wave height, incident wave height upon arriving in the vegetation canopy, the exponential decay coefficient, and the distance from incident wave, respectively.

Nevertheless, the seagrass blade's horizontal velocity and its interaction with the orbital velocity had to be understood where the blade's motion can reduce the drag force exerted on the vegetation. Some other studies though accounted for the flexible vegetations by adopting different materials to create artificial seagrasses. (OTA, KOBAYASHI, & KIRBY, 2005) used polyester blades with stem density of 1000 stems/m^2 long as half of the water depth in the flume and reported the wave attenuation below 10%. Another one (Bouma et al., 2005) compared stiff and flexible vegetation behaviours throughout their laboratory experiments on regular wave simulation. They concluded that the rigid vegetation exerts the highest drag led to wave dissipation around three times stronger than the flexible plants. Lima et al tried nylon strips to create seagrass simulating real seagrass motion behaviour at the laboratory tests. Reported results read 2.5 – 15 % of wave height reduction for plant densities 400 – 1600 stems/m^2 (Lima, Neves, & Rosauro, 2007). Varying results of wave height reduction and wave energy dissipation from laboratory studies led to some field projects to validate the laboratory tests. Bradley and Houser (Bradley & Houser, 2009) conducted a field study in northern Florida where seagrass canopies are found in shallow waters up to three meters of depth. They measured the wave heights using pressure transducers distributed exponentially complying with the extensively used exponential wave decay model (eq. 2.17) at different distances from the edge of the meadows shoreward. To tackle the relative velocity between seagrasses and oscillatory flow, the leaves' motion was assumed to be similar to a cantilever beam behaviour. Their result confirmed that the vegetation lay down along the flow direction for a longer time within the wave cycle when incoming wave heights increase that meadows are deemed the equivalent of a rigid body. Low-frequency waves had seagrasses moving in phase while for high-frequency waves leaves' motion was not in phase justifying the observed wave attenuation in the latter. They stated that, moreover, in low energy conditions, dissipation is subject to relative blade motion. As for deeper waters, Infantes et al. carried out a field study northeast of Mallorca, Spain where seagrass meadows are quite abundant at 6-35 meters of depth (Infantes et al., 2012). They deployed pressure sensors right above the canopies between 6-16.5 deep in the water within around 1 km seawards normal to the coastline. Their approach, however, was to calculate a bottom equivalent roughness, for the seabed covered with seagrasses, through which in turn, wave friction and attenuation are obtained. They eventually reported a wave height reduction of 50 % for waves with 1.1 metres height propagating over seagrass meadows with 600 shoot/m2.

In more recent studies, large-scale lab experiments were of interest to scholars being closer to the real conditions. Stragikaki et al. conducted large-scale lab experiments simulating regular waves and seagrasses interactions for intermediate and shallow waters for two different plant densities in three different water depths (Stratigaki et al., 2011). They adopted a 1:1 scale such that the analysis would not be influenced by scaling factors. For the plants, they used polypropylene stripes with different lengths in a PVC cylinder as the stem which emerges out of the bed a few centimetres. They took the advantage of resistive and acoustic wave gauges mounted within the flume to record wave heights; a flume of dimension 100 × 3 × 5 m. Following a set of 15 wave simulation tests, they concluded that the wave height reduction, as a wave attenuation indication, increases with vegetation density and submergence ratio (plants height/water depth). Later, Manca et al. (Manca et al., 2012) used the same flume and artificial seagrass design as (Stratigaki et al., 2011) to perform sets of regular and irregular wave simulations in order to make a comparison. They dedicated some experiments to unvegetated bed conditions as the controlled tests. They applied the common exponential decay model for wave attenuation as well meanwhile confirming that wave height reduces significantly by the seagrass meadows in both regular and irregular wave simulation tests.

Most of the studies applied the Kobayashi exponential model (eq. 2.17) to express wave decay while in higher velocities and subsequently higher Reynolds number, where quadratic drag law governs the drag force, the linear model derived by Dalrymple et al. (eq. 2.15) is more adequate (Luhar, Infantes, & Nepf, 2017).

Furthermore, being significantly flexible, seagrasses experience considerable deformation called "reconfiguration" which appeared not to be consistent with the linear beam theory based on the motion of the blades observed in another study (Luhar et al., 2017). Hence adopting cantilever beam theory, used in the majority of relevant studies, might not be sufficient to describe the reconfiguration's impact on the drag force experienced by the blade. To overcome this, they used an effective blade length responsible for wave dissipation based on the Cauchy number and the ratio of blade length to wave excursion_blade length ratio (Luhar & Nepf, 2016). Having considered these, they further conducted wave-seagrass interaction simulation experiments in a flume and reported that wave attenuation increase by increasing the vegetation density and the submergence ratio. Similar criteria were adopted by Lei and Nepf to propose a model predicting wave attenuation due to seagrass meadows taking into account the plant's morphology and density as well as the blade motion following a set of lab experiments (eq. 2.23) (Lei & Nepf, 2019). They also compared their model to some other major studies results from both in laboratory and field works and reported a suitable agreement between them.

Hence an effective blade length (l_e) which is the length of the blade contributing to drag force is obtained through the following equation.

$$\frac{l}{l_e} \sim (C_a L)^{-1/4} \tag{2.18}$$

Where l, C_a, and L in turn represent the blade total length, the Cauchy number, and the blade length ratio.

Given the flexible vegetation, blades move in the water resulting in a relative velocity between the water and blades while it is not equal to wave's horizontal orbital velocity. Thus, the wave energy dissipation rate due to the flexible plants is given by equation 2.19 (Lei & Nepf, 2019).

$$E = \frac{1}{T}\int_{t=o}^{T}\int_{z=0}^{l}(\frac{1}{2}\rho C_D a_v u_R|u_R|u\ dz\ dt) \tag{2.19}$$

Where a_v is the vegetation frontal area defined as the blade width multiplied by the blades per bed area times the plant density in the bed area and u_R is the relative velocity. Thus, the solution for equation 2.19 is given as

$$\frac{a}{a_0} = \frac{1}{1 + K_D a_0 x} \tag{2.20}$$

Where K_D is the dissipation coefficient obtained as

$$K_D = \frac{2}{9\pi} C_D a_v k \alpha^3 \frac{9\sinh(kl) + \sinh(3kl)}{\sinh\ \mathrm{kh}(\sinh(2\mathrm{kh}) + 2\mathrm{kh})} \tag{2.21}$$

Where α accounts for wave velocity reduction in the canopy.

Lei and Nepf, following the blade effective length scaling law, proposed a relationship to calculate the effective meadow height ($l_{e,m}$) accounting for the wave dissipation coefficient for seagrass meadow (Lei & Nepf, 2019).

$$l_{e,m} = 0.94(Ca_w L)_b^{-0.25} l_b + l_r \tag{2.22}$$

Where l_b and l_r are the flexible and rigid length of the blade length l, respectively. It should be noted that both the Cauchy number (Ca_w) and blade length ratio (L) are to be obtained using the blade flexible length (l_b).

Eventually, by substituting $l_{e,m}$ with l in equation 2.21, their proposed model for wave dissipation coefficient due to seagrass meadow reads

$$K_D = \frac{2}{9\pi} C_D a_v k \alpha^3 \frac{9\sinh(kl_{e,m}) + \sinh(3kl_{e,m})}{\sinh\ \mathrm{kh}(\sinh(2\mathrm{kh}) + 2\mathrm{kh})} \tag{2.23}$$

Chapter 3

Methodology

3.1 Seagrass meadow design and manufacturing

The first step was to design and manufacture artificial seagrasses mimicking the natural plant's behaviour while interacting with hydrodynamic forces to a reasonable extent. Most importantly, the plant’s mechanical properties i.e., stiffness, and leaf cross-sectional area, are the underlying factors to be considered. Seagrasses are clonal meaning that a horizontal or/and vertical stem called a “rhizome” hold several plants each composed of a bundle of leaves called a “shoot” (fig 3.1). Varied with different species, each plant may have between 2-10 leaves that are maintained together by the “sheath”_ a transition segment from the rhizome to the leaves (Hemminga & Duarte, 2000).

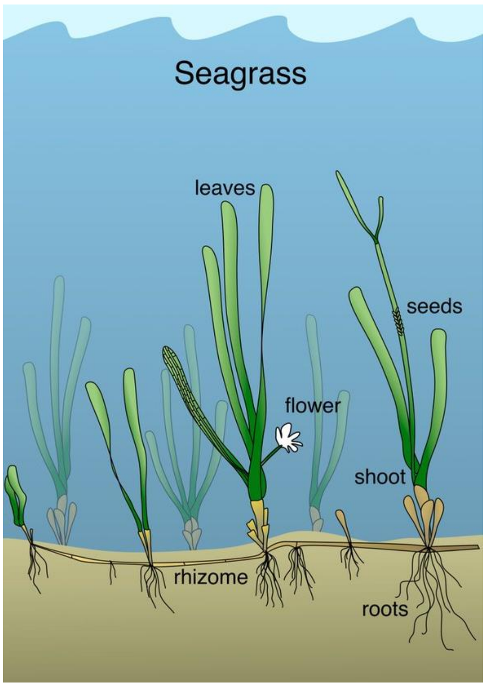

Fig 3.1. schematic of seagrasses (www.seagrasswatch.org)

In order to create the seagrass model in the laboratory, field data of seagrass different species (de los Santos et al., 2016) was used to perform dimensional analysis such that using dimensionless parameters proper down-scaled properties of the leaves required for the plant model are obtained. The plant leaves' motion underwater is of concern whose governing characteristic is predominantly the drag force which can take different values based on the Cauchy number (C_a) which is the ratio of hydrodynamic drag to the restoring force exerted from the leaf (blade), the buoyancy parameter (B) which is the ratio of restoring forces due to buoyancy to the stiffness of the blade, the blade length ratio (L_b) that represents the blade's length over the wave excursion, the meadow length ratio (L_m) given as the meadow height on the wavelength, the velocity ratio (U_r) representing the current velocity over wave orbital velocity, and the meadow porosity or density (φ). However, the buoyancy parameter, being too small (Luhar & Nepf, 2016), and the meadow length ratio both have a negligible contribution and since we are not considering current, the blade Froud number (Fr) which is the ratio of mean horizontal wave orbital velocity to the square root of gravitational acceleration and the blade length product is deemed instead of the velocity ratio. Consequently, the drag force is a function shown in equation 3.1 followed by other equations describing the overmentioned dimensionless parameters.

$$F_d = f(C_a, L_b, Fr_l, \varphi) \tag{3.1}$$

$$C_a = \frac{\rho b U^2 l^3}{EI} \tag{3.2}$$

$$L_b = \frac{l}{A_w} = \frac{2\pi l}{UT} \tag{3.3}$$

$$Fr = \frac{U}{\sqrt{gl}} \tag{3.4}$$

Where ρ is the water density, b is the blade thickness, U is the horizontal wave orbital velocity, l is the blade length, E is the Young modulus, A_w is the wave excursion, T is the wave period, and g is the gravitational acceleration.

As argued before, scale ratios between the real plant's leaf and the model's blade for different properties can be obtained using the dimensionless parameters above. Thus, these parameters are equalised for the real plant and the model condition. In the following an example is provided of how dimensional analysis was carried out.

$$Fr_p = Fr_m \rightarrow \frac{U_p}{\sqrt{gl_p}} = \frac{U_m}{\sqrt{gl_m}} \rightarrow$$

$$\frac{U_p}{U_m} = \frac{\sqrt{gl_p}}{\sqrt{gl_m}} \rightarrow \text{given the equal gravitational acceleration, it reads} \rightarrow$$

$$velocity\ ratio = \sqrt{length\ ratio}$$

Eventually, having the mechanical and morphological properties of the seagrass leaves (table 3.1), the corresponding seagrass model characteristics were obtained with length, thickness, and width of 100 mm, 0.09 mm, and 2 mm, respectively with Young's modulus of 128 MPa. As for the leaves, blades thence, polyethene strips with the abovementioned properties have been used thereby four blades comprised of each plant bundled using polypropylene shrinkage tubes as the stem (fig 3.2).

Table 3.1 Seagrass mechanical and morphological properties

Species	t (mm)	w (mm)	l (m)	E (MPa)	Submergence ratio (l/h)	Number of leaves
C. nodosa	0.1-0.4	2.6-4.7	0.1-0.55	55-105	0.1-1	4
P. oceanica	0.2-0.5	9-10.8	0.15-0.75	110-470	0.02-0.5	7
Z. marina	0.15-0.44	3-12	0.15-0.8	100-380	0.1-0.5	4
Z. noltii	0.16-0.26	1-2.7	0.05-0.27	75-1000	0.1-1	4

Fig.3.2 plants model setting in plexi glass baseboards

Further, to have a wide range of plant density and considering the flume dimensions, four different patterns consisting of 251, 502, 669, and 1338 plants/m^2 from scarce to dense configurations were considered, respectively. However, to uphold the plants while submerged in the water, mimicking the natural seagrass meadows with roots buried in the seabed, a set of four plexiglass boards were drilled, thus in line with all density patterns. Figures 3.3.a and 3.3.b represent an example of the drilled base board and when it is deployed by the plants, respectively.

(a)

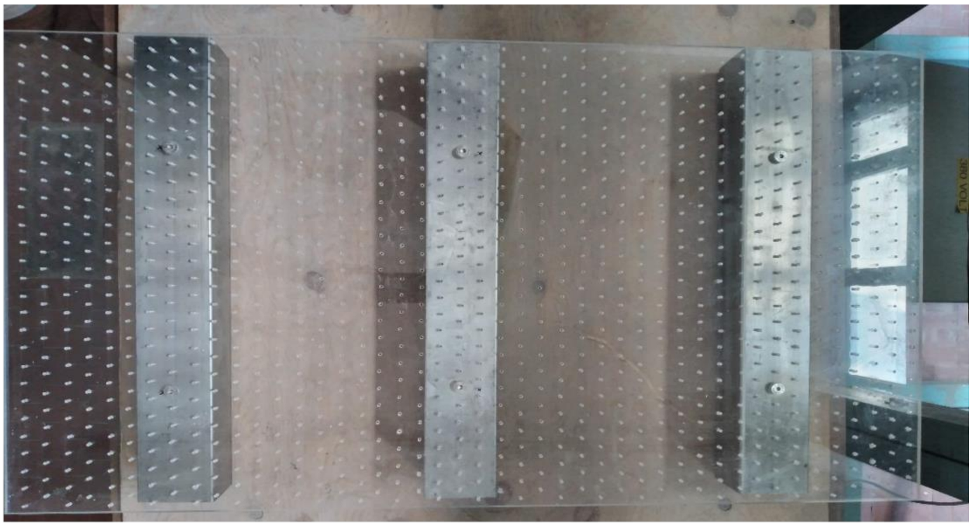

(b)

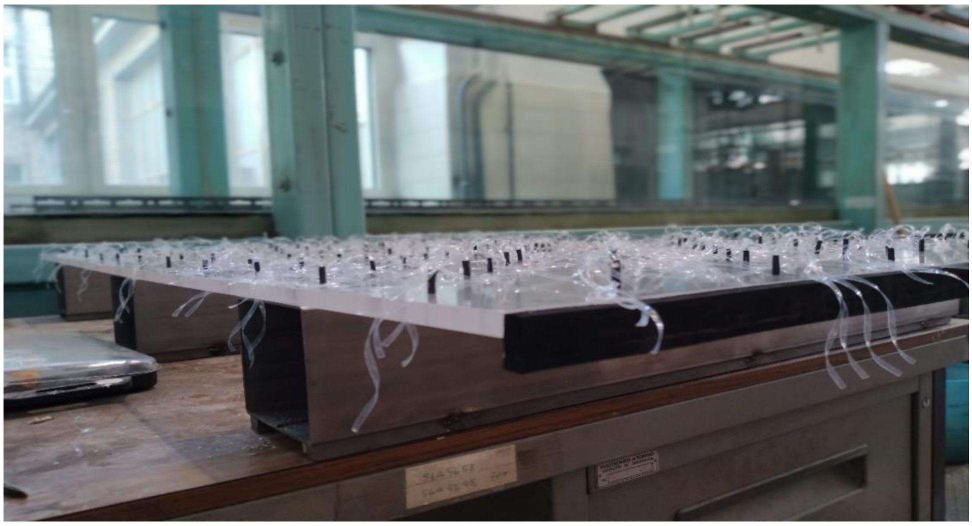

Fig 3.3 (a) Plexiglass baseboard and drilling configuration, (b) plants deployed in the baseboard

3.2 Wave design and characteristics

As for the water depth and wave characteristics, we meant to cover the water depths which real seagrasses inhibit while imposing a broad range of regular wave conditions on them. However, given the flume dimensions and functioning limits, various water depths and wave heights along with an appropriate submergence ratio were evaluated in order to examine the feasibility of providing such hydrodynamic conditions in the flume. Finally, wave heights roughly ranging from 0.01 to 0.18 m in water depth of 0.15 to 0.6 m were deemed to properly address the study goals. A total of 66 experiments were designed by varying water depth, wave height and wave period (the wave characteristics for all experiments are reported in appendix A). all the experiments were conducted with an unvegetated bed, as the benchmark experiments, and vegetated bed for each plant density.

3.3 Hydraulic conditions

The experiments were performed in the wave flume at the hydraulics and fluid mechanics laboratory of the Politecnico di Torino. A 46-metre-long fixed-bed channel with 0.6-metre width and 1-metre depth. The flume is equipped with a piston wave maker through which the designed waves can be generated (fig3.4.a). At the end of the flume, a parabolic absorbent beach is designated which can be displaced vertically anticipating minimum reflection (fig 3.4.b).

(a) (b)

Fig 3.4 The wave flume and (a) wavemaker and its (b) embedded beach at DIATI, PoliTo

3.4 Instruments

Wave attenuation can be estimated by means of wave height variation before, along, and after the meadows. This, however, being a delicate evaluation given the wave intrinsic features, requires adequate measuring instruments proposing quite a reasonable precision. Water level measurement methods vary from hydrostatic measurement devices, such as displacers, bubblers, differential pressure transmitters, resistance/conductive sensors etc., to modern technologies such as Magneto strictive, ultrasonic, laser, and radar level transmitters. As long as precision is concerned, a point-level measurement would be preferred, and resistance sensors are one of them through which water resistivity is measured and proportionally the water height too.

The “WG8USB” wave gauges produced by “Edinburgh design” were employed in this study. The system used includes a set of eight resistance wave gauges each consisting of two parallel stain steel rods connected to the electric current from the top. The resistivity between two rods is computed by the sensors which are proportional to the water height. The sampling frequency can be selected as 32, 64, 128, and 256 (Hz) which are quite sufficient compared to the real sea wave frequencies. Using a USB hub interface, they are connected to the PC where digitized data logs are recorded as text files. Though to evaluate the efficiency of the wave gauges, a set of seven ultrasonic sensors produced by “Balluff company” were used so that their measurement could be compared to the resistant gauge ones in order to select the most efficient tool given this study's goals. Ultrasonic sensors require no contact with water to perform the measurement. The sensors emit ultrasound waves towards the water's surface and the travel time in between is measured. Once the reflected sound waves arrive at the sensor, the distance (water level) is calculated given the velocity and travel time of the sound waves. The opted ultrasonic sensors can operate within 15 cm from the water surface for optimal results and their transducer frequency is 380 kHz. However, we should note that ultrasonic sensors conduct continuous measurements, unlike point-level measurements i.e. resistance wave gauges.

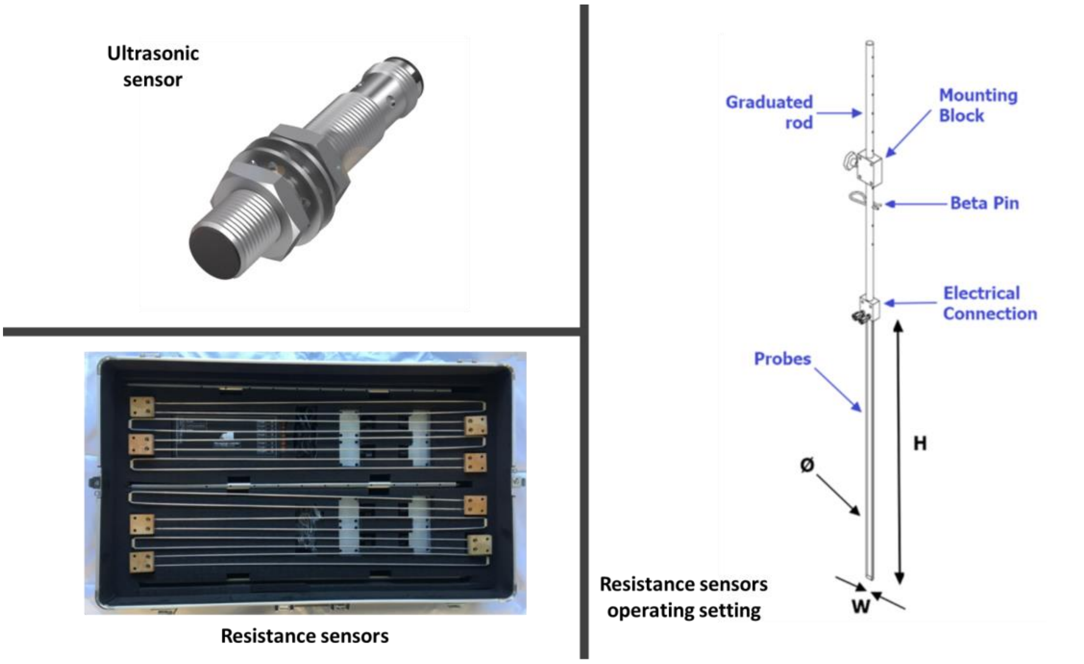

Fig 3.5 Ultrasonic and resistant sensors used in this study

3.5 Data analysis

The free water surface time series recorded by the resistance wave gauges (wg) were checked whether they are in line with the regular wave characteristics. Moreover, a transient range between the time that the wavemaker initiates to generate the waves and when the expected waves are fully developed had to be identified and removed. The same procedure was taken for the part of the time series associated with the reflection effect from the beach at the end of the flume by calculating the time required for the waves reflected to arrive at each wg position.

After that, having the mean wave height (amplitude) in each experiment calculated using equation 2.4, we can obtain the dissipation coefficient K_D at the position of each wg through equation 2.20 where a_0 is the wave amplitude at the wg1, being located before the meadow, a is the wave amplitude obtained at the wave gauges over the meadow (wg 2-7), and x is the distance from the wave gauge 1. Given that K_D for all wave gauges of interest is obtained based on a similar reference point (wg 1), a linear regression can provide us with a single K_D for each experiment with a limited error propagation rather than taking an average between all the values. It should be noted that the dissipation due to the flume bed was removed from the total K_D subtracting values from the benchmark experiments to the others in order to obtain the pure plant's dissipation contribution.

The final step was to obtain values provided by the model to make a comparison. First, $l_{e,m}$ was obtained using equation 2.22. However, the drag coefficient in equation 2.23, representing the rigid part of the plant, should account for both the stem and the constrained portion of blades. Therefore, given the relationship proposed by Lei and Nepf, $C_{D,stem} l_{stem} d = C_D 4 b l_{stem,e}$ where d is the stem width, b is the blade width, and $l_{stem,e}$ is the stem effective length, thus the rigid length l_r required to calculate $l_{e,m}$ is modified proportionally. Eventually, the values for the prediction model for each experiment were calculated through equation 2.23 and compared with the estimated values from the experiments performed in this study.

3.6 Preliminary experiments

Prior to the main experiments, a set of preliminary experiments (table 3.2) for a wide range of wave heights was conducted in order to attain the following goals and hence the final experimental setup.

- Sensors functioning verification
- Definition of the wavemaker transfer function

Table 3.2 Preliminary experiments hydrodynamic & hydraulic detail

Experiment n◦	Wave Frequency (Hz)	Expected wave height (m)	Water level (cm)
1	125	0.04	0.46
2	0.62	0.06	0.46
3	125	0.08	0.46
4	0.62	0.08	0.46
5	0.84	0.10	0.46
6	0.84	0.12	0.46
7	125	0.16	0.46
8	125	0.01	0.46
9	0.62	0.02	0.46
10	0.84	0.03	0.46
11	0.84	0.05	0.46

3.6.1 Sensors functioning verification

As discussed earlier, both the resistance and ultrasonic sensors were tested in order to evaluate and compare their performance such that the most efficient one is selected given this study's objectives. Each pair of sensors (seven each) were positioned adjacent to each other so that the recorded wave heights will be almost in the same range. To install and mount the sensors along the flume, heavy steel profiles were opted perpendicular to the flume length to support the sensors guaranteeing their stability during the experiments. This is shown in the following figure and the whole setup concept is elaborated in the schematic figure 3.7.

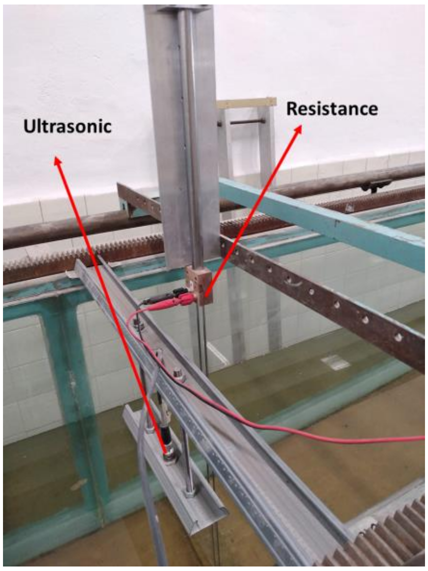

Fig. 3.6 Ultrasonic and resistant sensors configuration

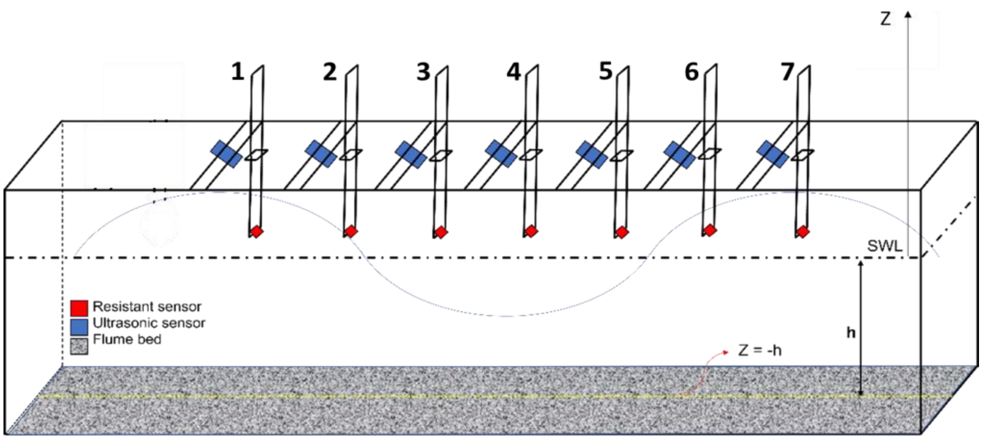

Fig. 3.7 Schematic configurations of the sensors over the flume-preliminary experiments

As a comparison indication, the difference between wave heights, obtained through equation 2.4, detected by the resistance and ultrasonic sensors within each experiment (ΔH) was obtained where figure 3.8 elaborates the result for wavelength (λ) and wave steepness (H/λ) at each paired sensor position defined in figure 3.7. It is observed that the sensors do not provide quite a similar result, especially, when it comes to the waves characterised by the larger steepness and, hence, affected by stronger instability. Given the continuous-detection performance from ultrasonic sensors compared to the point-level accuracy provided by the resistant one, the inconsistency in results is acknowledged. Yet ensuring a compelling performance concerning the study resolution is of great importance. Thus, the obtained water surface time series were observed having them plotted in 2-D figures. Figure 3.9 represents experiment number seven featuring the highest wave height as an example being the worst possible discrepancy between sensors' performance.

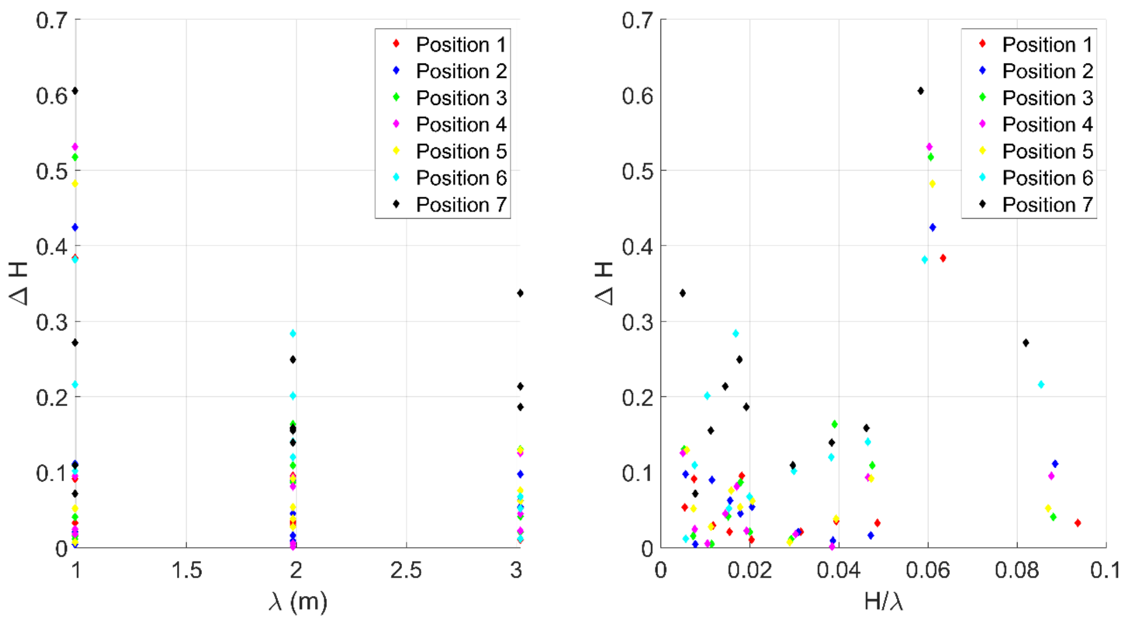

Fig. 3.8 Normalised mean wave height difference against wavelength (L) and wave steepness (H/λ)

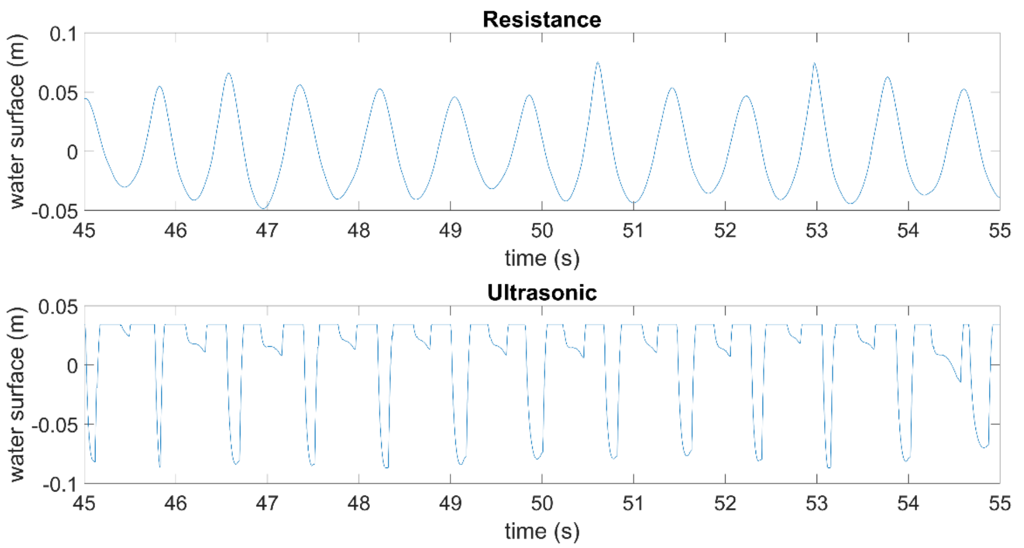

Fig. 3.9 experiment 7-sensors pair 7 free water surface time series

we can appreciate that ultrasonic sensors did not have a reliable performance for such a large wave height while the resistant sensors' result seems appropriate. However, the waves are not monochromatic as expected which will be addressed and discussed in wavemaker specific section. The first experiment also, showing the second-largest mean wave height difference, is worth assessing (fig. 3.10). In this case, too the resistant sensors demonstrate reliable performance, unlike the ultrasonic ones within which are there minor distortions in the recorded times series.

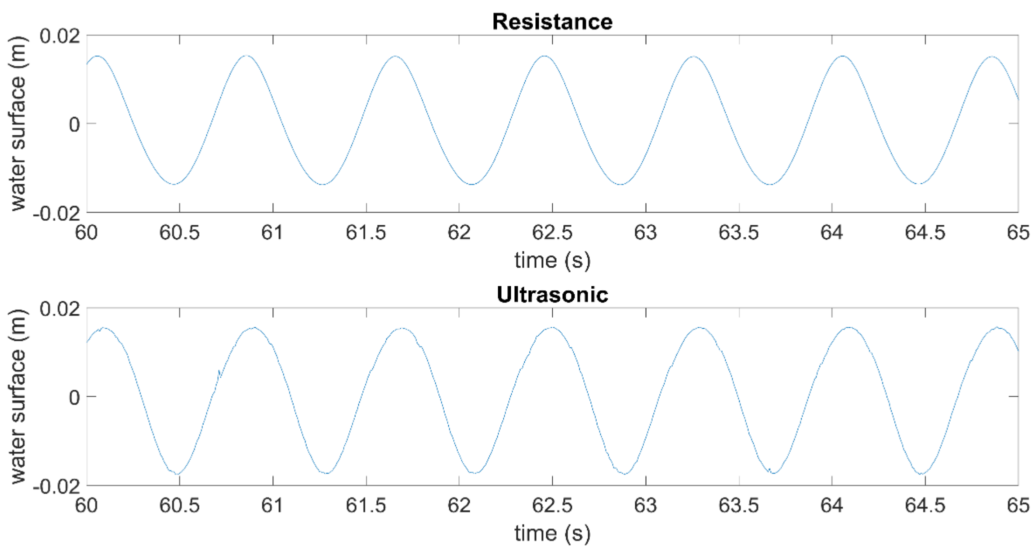

Fig. 3.10 experiment 1-sensors pair 7 wave time series

As a final check, the experiment time series with the lowest wave height (fig. 3.11) was assessed too so that a prudent decision about the sensors' performance would be expected. In this case, likewise, the ultrasonic sensors' recorded time series are associated with distortions whereas resistant sensors' record is vividly trustworthy. The resistant sensors hence are selected for the main experiments and the final configuration of the sensors is represented by figure 3.12 where numbers denote the order of wave gauges in use in this study.

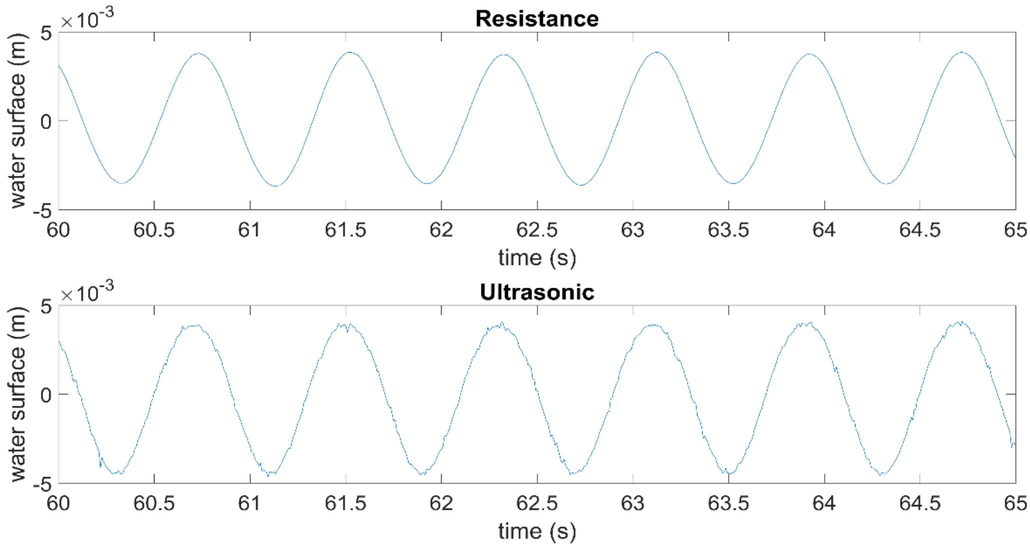

Fig. 3.11 experiment 8-sensors pair 7 wave time series

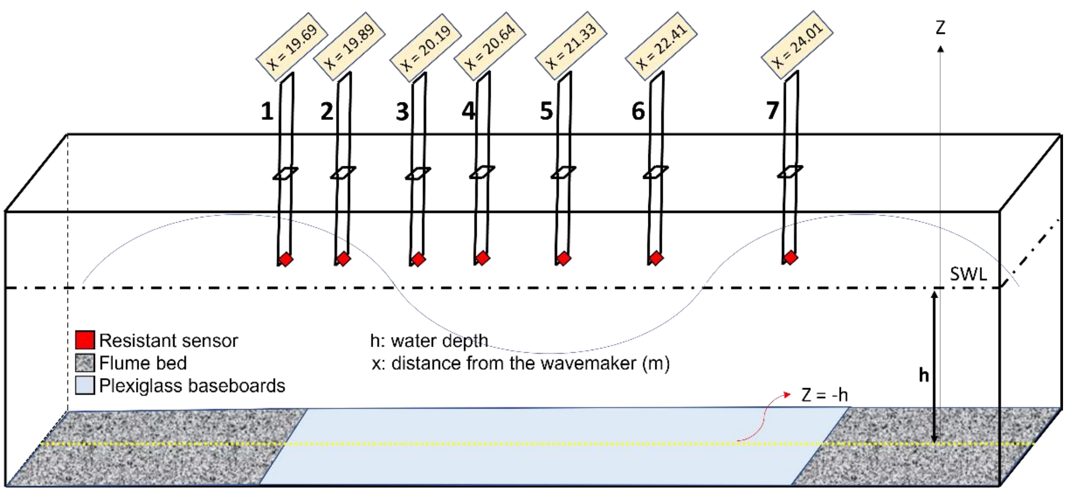

Fig 3.12 Schematic configurations of the sensors over the flume-main experiments

3.6.2 Wavemaker transfer function

The waves had to be generated by the piston-type wavemaker located at the beginning of the flume. The wave characteristics of interest are input into a programme script written in Matlab which commands the wavemaker to initiate wave generation. Each wave requires a specific voltage used by the wavemaker in order to be generated and this is provided by a transfer function to be determined for the wavemaker in use applying the wavemaker theory developed by Galvin for shallow water (Galvin, 1964).

Based on the theory, the volume of water underneath the wave crest is equal to the water displaced by the wavemaker. The piston wavemaker displacement range, which is horizontal, called stroke, is denoted by *S* which times the water depth *h* gives the displaced volume of water by the wavemaker (fig. 3.13). The volume of water below the crest is $\int_0^{\lambda/2} \frac{H}{2} \sin(kx)\, dx = \frac{H}{k}$ and is equal to *Sh*. Eventually, this gives the ratio between wave height (*H*) and piston wavemaker stroke (*S*) for shallow water ($kh < \pi/10$) as follows.

$$\frac{H}{S} = kh \tag{3.22}$$

This can be expressed as well for a wide range of water depths

$$\frac{H}{S} = \frac{2(\cosh 2kh - 1)}{\sinh 2kh + 2kh} \tag{3.23}$$

Figure 3.14 elaborates on wave height to stroke ratio in different water depths.

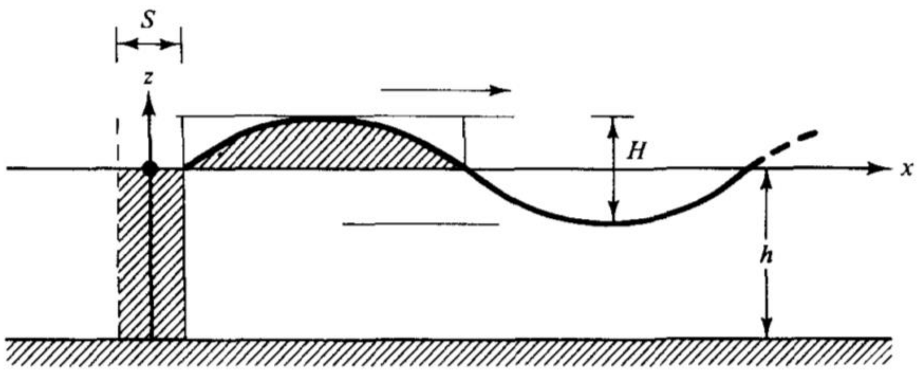

Fig. 3.13 shallow water piston-type wavemaker theory of Galvin [Dalrymple 1984]

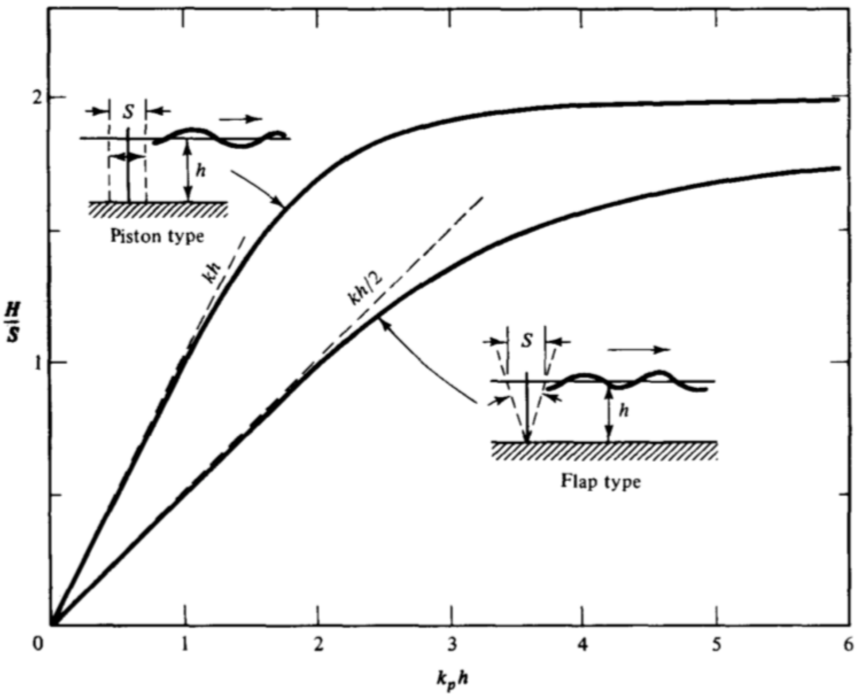

Fig. 3.14 plane wavemaker theory [Dalrymple 1984]

However, in practice, the stroke range values (*S*) might not be available a priori while, being a function of *kh,* the ratio between the wave height and voltage (*H/V*) represents the same behaviour as (*H/S*)_ i.e., *H/V = H/S * S/V*. Having data, particularly voltage values, from other experiments conducted using the same wavemaker along with another set of preliminary experiments carried out for this study, where a series of voltage values gave their corresponding wave heights, we managed to estimate a polynomial transfer function for the wavemaker. Figure 3.15 demonstrates the resultant *H/V* for different *kh* values.

$$\frac{H}{V} = -2.10E^{-7} + 3.71E^{-6}kh - 2.04E^{-6}kh^2 - 4.26E^{-4}kh^3 + 0.004kh^4 - 0.02kh^5 + 0.05kh^6 - 0.01kh^7 \tag{3.24}$$

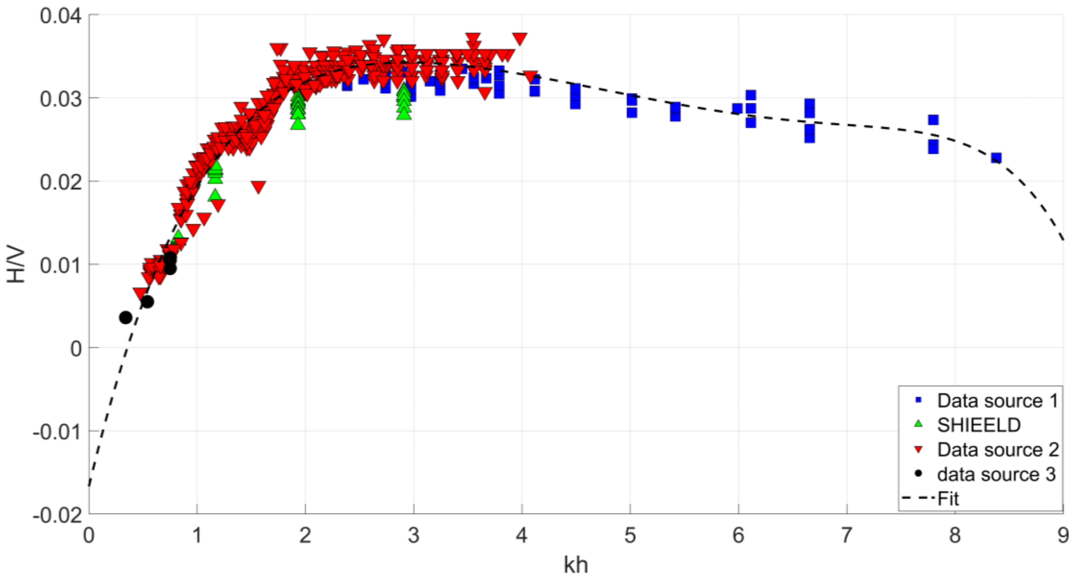

Fig. 3.15 the value of H/V as a function of kh for data from various sources and the wavemaker transfer function obtained as the best fit for a polynomial regression.

We can observe that, as long as shallow water is concerned, there is a good agreement between theory and field results while for higher water depths a mismatch is witnessed which could be possibly related to the wavemaker limits and range of functioning.

Chapter 4

Results

Wave heights recorded by the resistance wave gauges during each experiment were post-processed and manipulated according to the procedure described in section 3.5 in order to prepare data in the context of linear wave theory to assess the seagrass effects on the wave height as the first objective of this study. In the majority of cases, wave trains represent regular wave characteristics quite well_i.e., a sinusoidal behaviour. However, in water depths 15, and 20 cm for wave frequency below 0.7 and 0.6 Hz, respectively, it appears the wavemaker is not able to show a very well performance as long as the linear wave framework is concerned. This can be seen in figures 4.1-4.3 where in turn instances of wave trains for water depth 15, 20, and 60 cm recorded by the wave gauge 3 during the benchmark experiments are shown. Water depth of 60 cm was selected to demonstrate appropriate performance of the wavemaker in higher water level.

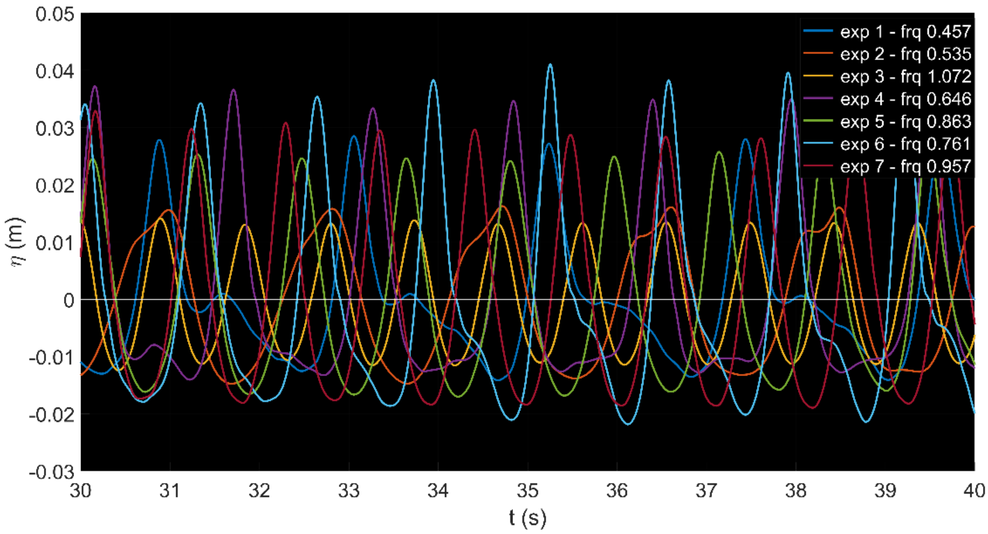

Fig. 4.1 Wave time series for benchmark experiments-water height 15 cm

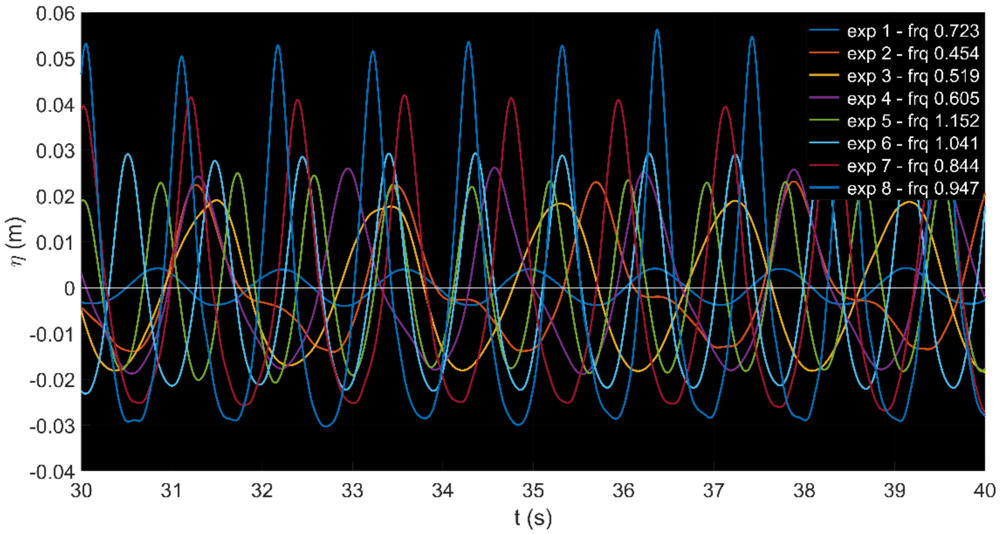

Fig. 4.2 Wave time series for benchmark experiments -water height 20 cm

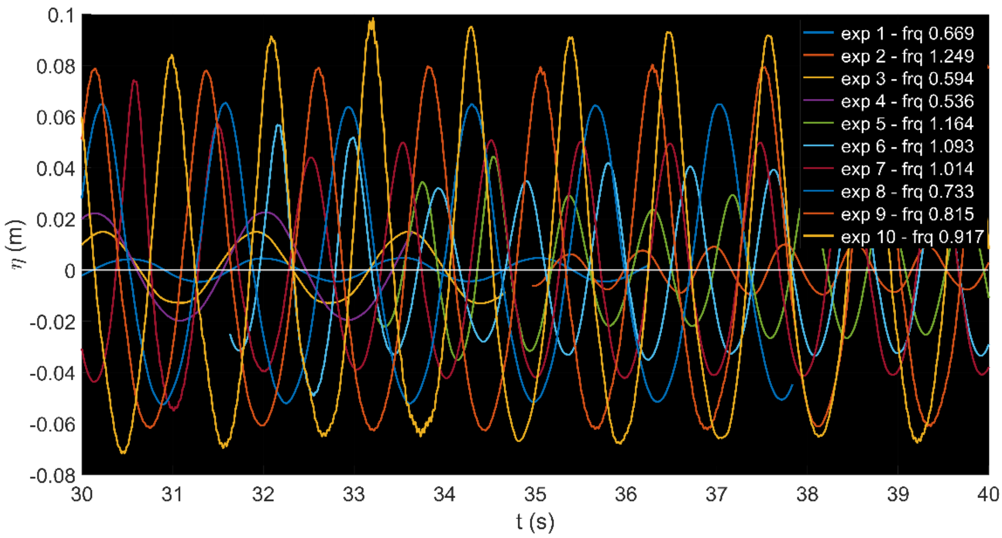

Fig. 4.3 water surface time series for benchmark experiments -water height 60 cm

Having the clean and trimmed data, the dissipitation coefficient (K_D) was obtained for each experiments and plant density and are demontrated by figure 4.4. As expected, it was observed that the dissipation increases with an increase in vegetation density, especially in lower water depths (i.e., 15, 20, and 30 cm) where this increase is well noticeable.

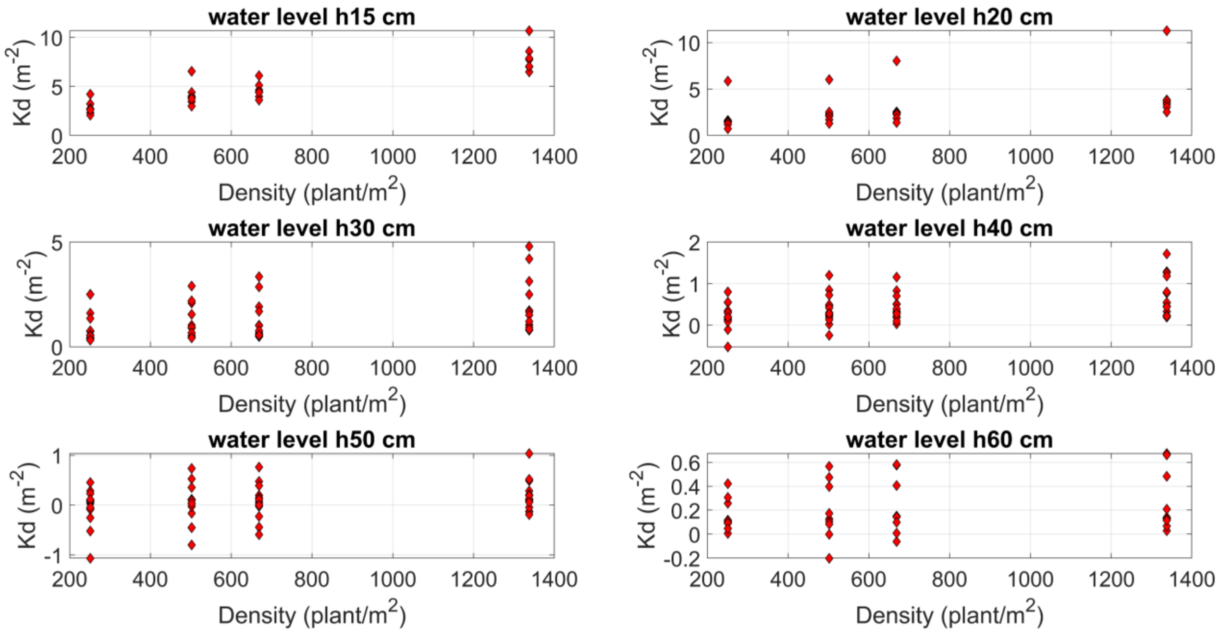

Fig. 4.4 estimated dissipation coefficient for different seagrass densities in water depths

Some negative values are observed starting from the water depth of 40 cm and they increase in number at the water depth of 50 cm. It appears that while the water level increases the seagrass effect on the wave height diminishes and in some cases the wave height remained unimpacted resulting in sort of similar values to the condition where no plants are involved. Moreover, close distance between the wave gauges could result in smaller diference between the wave heights recorded by two consecutive wave gauges (ΔH). Hence, it is not simple to resolve the real ΔH as its magnitude is comparable to that of the error, especially in high frequencies where most of the negative values are observed. Thus, a higher standard deviation may impact the accuracy of the linear regression.

As for the final step, the values of dissipation coefficient given by the predicting model were obtained to compare with the estimated values provided using the experimental data in this study. For comparison, the results were plotted against each other where a 1:1 scale line stands as the perfect match between them (fig 4.5).

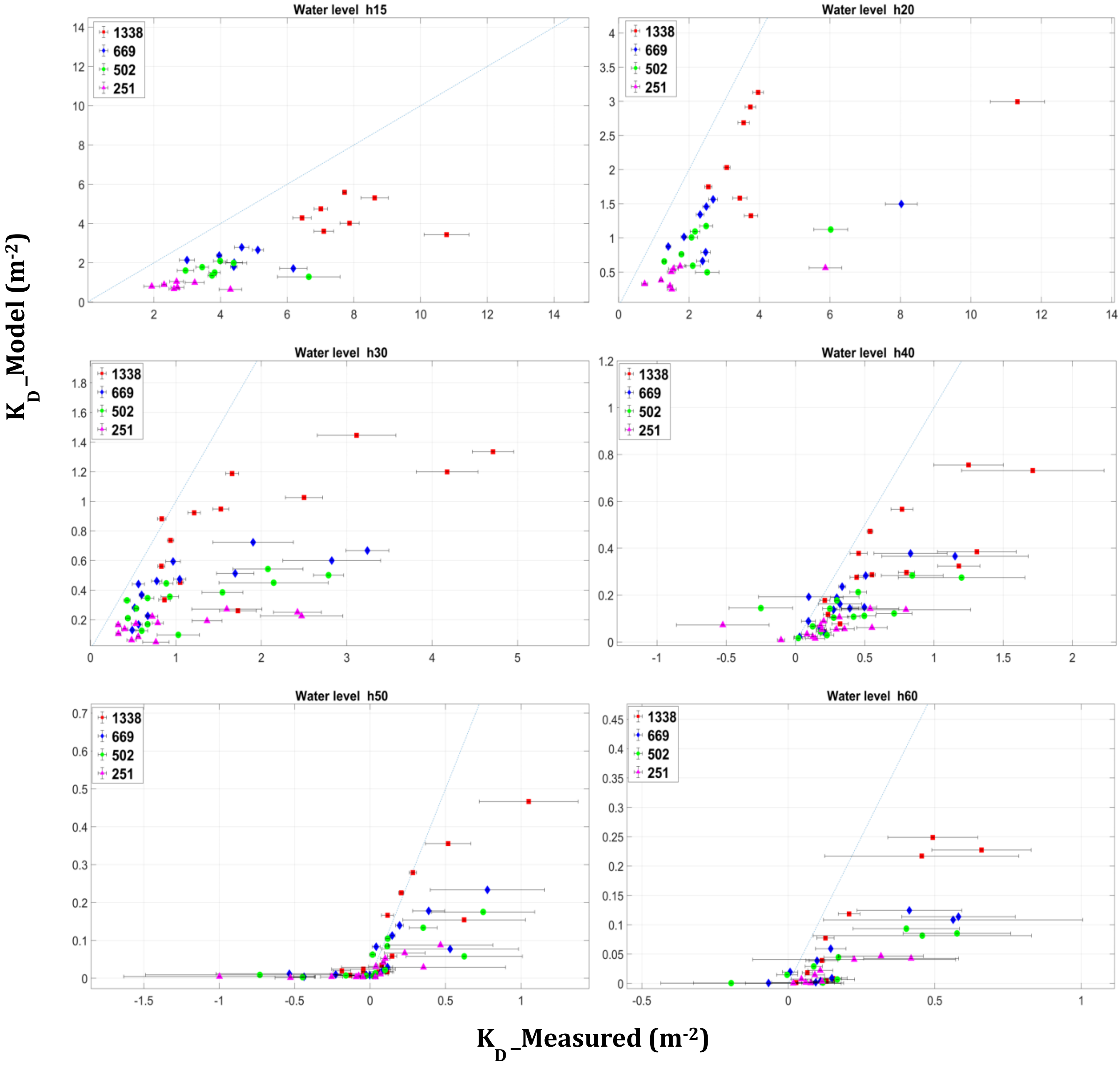

Fig. 4.5 K_D estimated vs. Predicted values - the dashed line denotes a perfect match between K_D measured and K_D predicted

A relatively good agreement is observed for individual experiments between the measured and predicted values. Nevertheless, for a constant water depth we can assess the compatibility using a linear regression between the estimated values and predicted ones and hence the following relationships are obtained for each water depth. Only in the water depth of 15 cm a relatively reasonable alignment is observed having a slope of 0.7 which is the closest one to unity compared to the other water depths.

Table 4.1 linear regression result between the measured and predicted k_D values

Relationship between K_D values (model vs. measured)	**Water depth (cm)**
$K_{D,model} = 0.7K_{D,measured}$	15
$K_{D,model} = 0.2K_{D,measured}$	20
$K_{D,model} = 0.22K_{D,measured}$	30
$K_{D,model} = 0.24K_{D,measured}$	40
$K_{D,model} = 0.11K_{D,measured}$	50
$K_{D,model} = 0.16K_{D,measured}$	60

Discussion

In order to understand the reason for cases where the measured values are too larger than the ones predicted by the model, it makes sense to check and compare the conditions in which the experiments were done for the predicting model and the present study. As for the hydraulic condition and the wave characteristics for our experiments and those provided in the prediction model by Lei and Nepf, Table 4.2 represents the range for some major factors.

Table 4.2 waves and hydraulic condition for the measured and predicted K_D values

Factor	Present study	Lei and Nepf
Water depth (cm)	15-60	18-45
Wave amplitude (cm)	0.5-8.5	0.8-5
Wave period (s)	5-13.7	1, 1.2, 2
Flume dimension (length x width cm)	46 x 60	24 x 38
Plant density (plant/m^2)	251-502-669-1338	280-600-850-1050-1370

We roughly can assume the difference between the values in the table 4.2 may contribute considerably to the final result for the K_D values reported in either of the studies. However, some other characteristics might have a significant contribution to the result. As for the very shallow water depths (h = 15, 20 cm), the very large measured K_D may attribute to presence of more than one harmonic within their corresponding wave train e.g. the first experiments done in h = 15 cm (Figure 4.5).

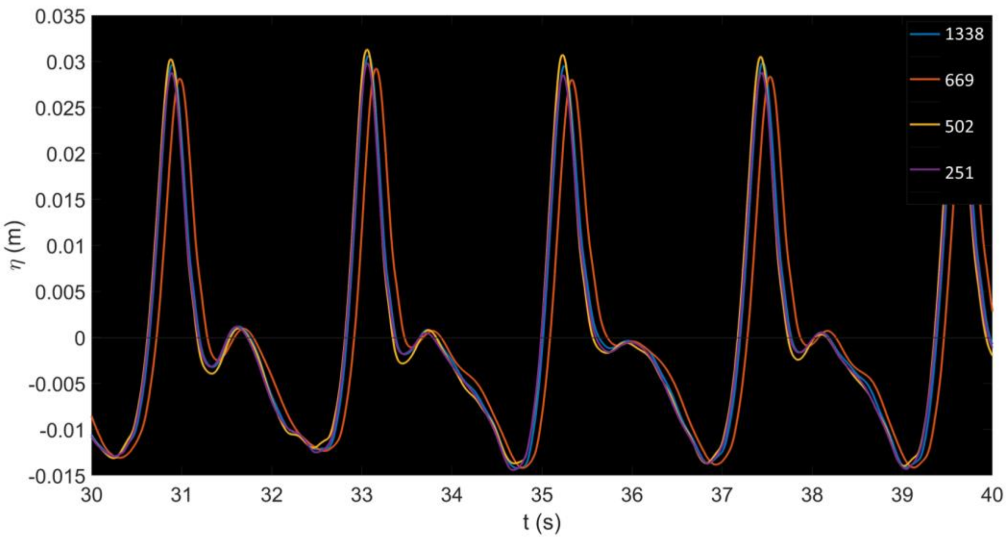

Fig. 4.5 water surface time series for experiment 1 -water height 15 cm

Another parameter is the wave excursion (A_w) that in shallow water depths (h = 15, 20 cm) appears to be important where on average its larger values led to a smaller difference between the measured and model values of K_D though this effect cannot be appreciated when water depth increases (fig 4.6). Increasing the wave height (H) leads to smaller K_D values that are closer to their corresponding ones predicted by the model (fig 4.7). Going up in water depth it is observed that the wave height variation impact on K_D diminishes but for the very small ones (i.e., H < 2cm) while the wavelength (λ) appears to affect K_D more (fig 4.8) where in some wavelengths the measured K_D values escalate standing far from the model's values. This, in fact, is due to another parameter wave steepness (H/λ) that for some wave heights varies between this study and that of the predicting model provides. In other words, given the two studies, although the wavelength range is quite similar, the wave height range used in this study encompasses a wider range than the other one and hence a wider range of wave steepness (fig 4.9).

The other significant variable that affects K_D values is the Cauchy number (C_a) which in our experiments ranges from 0.15 to 913.55 and is far smaller compared to the condition in which the prediction model was obtained where C_a is between 90 and 3800. This indicates that our seagrass model was stiffer thus higher K_D values were obtained. This is supported by the twisted shape of the blades, during our experiments, resulting in a larger moment of inertia (I) and this was taken into account while calculating the model values through equation 2.23 where C_a is required to obtain the seagrass meadow's effective length. Figure 4.10 elaborates K_D values' dependency on C_a where we can appreciate that for all water depths and seagrass densities, an increase in C_a results in lower K_D and thus a better agreement between the measured and model values.

In terms of velocity, the Keulegan-Carpenter number (K_C) is another dimensionless contributing factor that could explain the result and those cases where there is a large difference between the measured and model K_D values. K_C describes the importance of drag force relative to the inertia and is defined as $U \text{x} T \text{x} D^{-1}$ where U is the maximum wave orbital velocity, T is the period and D is the stem diameter of the plant. Given the constant diameter of the stem, variation in velocity and/or period changes the value of K_C which has an inverse relationship with the drag coefficient (C_D). Being constant the wave period during each experiment, it is the velocity which governs the K_C where for the present study it ranges from 0.0037-0.2954 m/s and that of providing the K_D model from 0.031-0.207. This implies that for very low velocity and smaller K_C, where C_D is higher, a large K_D is expected. This is another reason for some other cases with misalignment between the measured and model Kd values where with increasing K_C a good agreement is appreciated (fig 4.11).

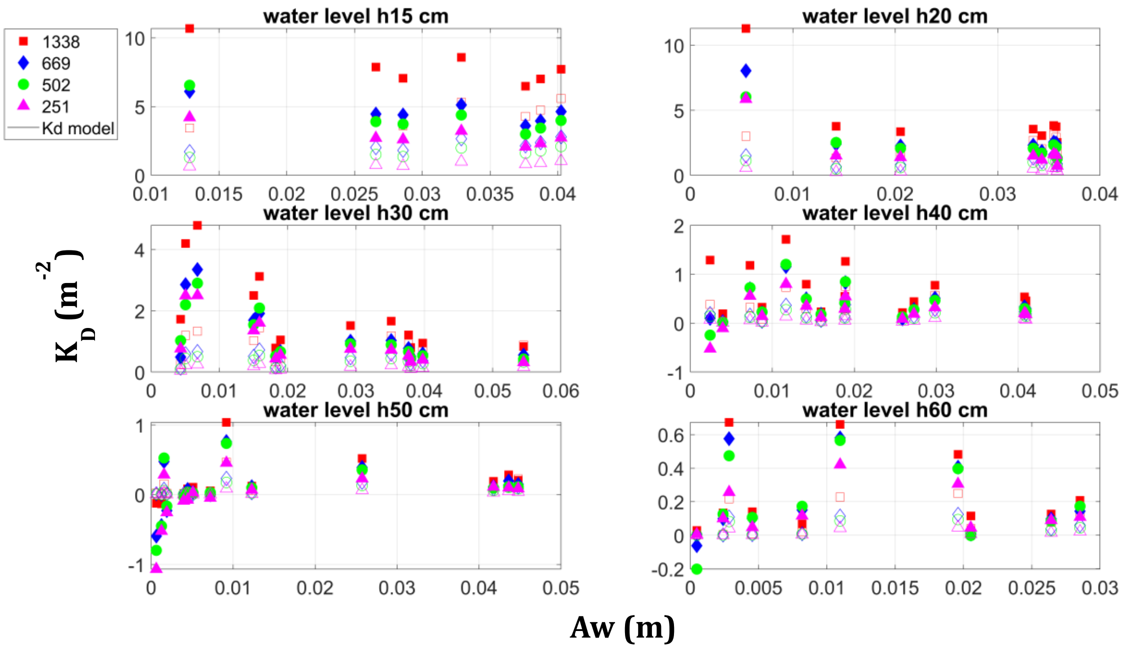

Fig 4.6 K_D values variation with A_w (at wg 7) for different water depths and seagrass densities

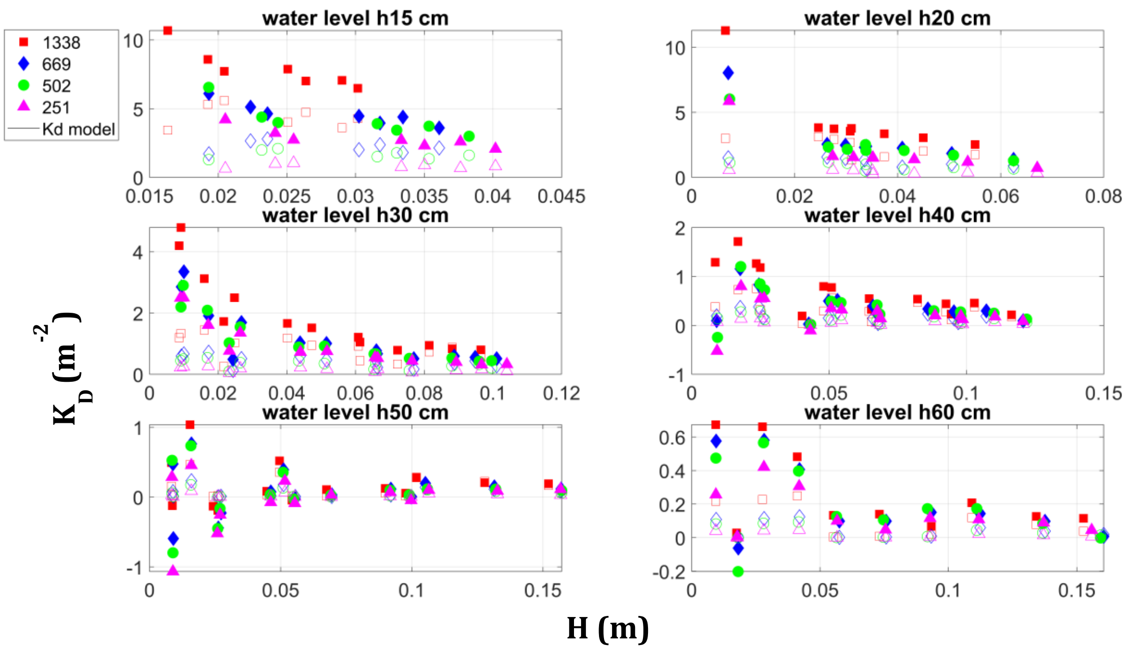

Fig 4.7 K_D values variation with H (at wg 7) for different water depths and seagrass densities

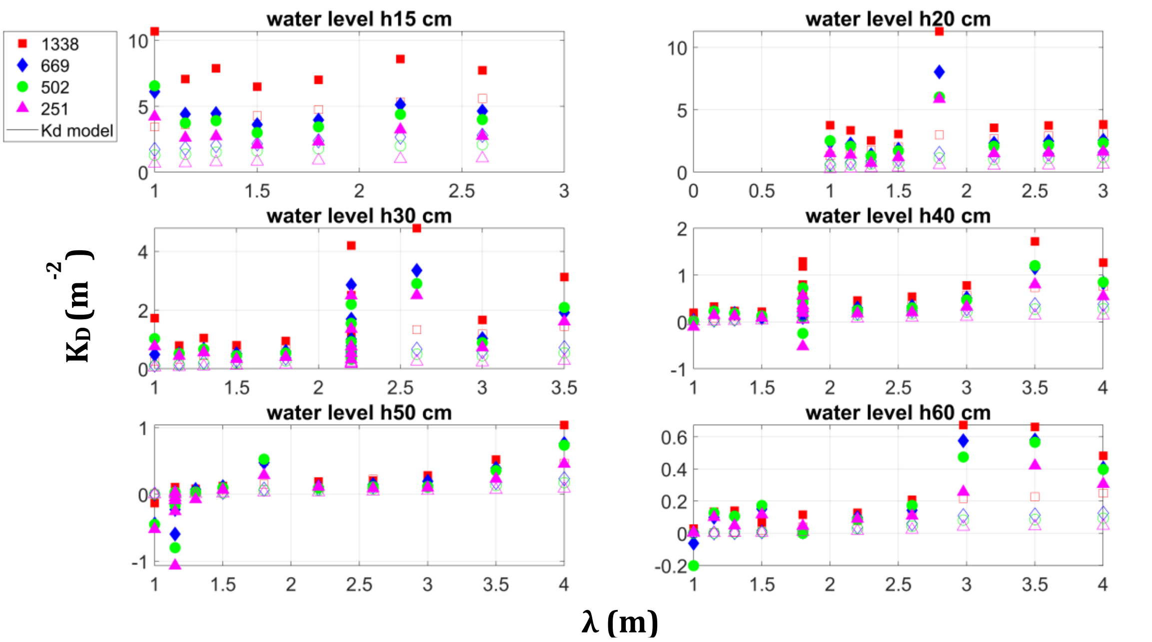

Fig 4.8 ***K_D*** **values variation with λ for different water depths and seagrass densities**

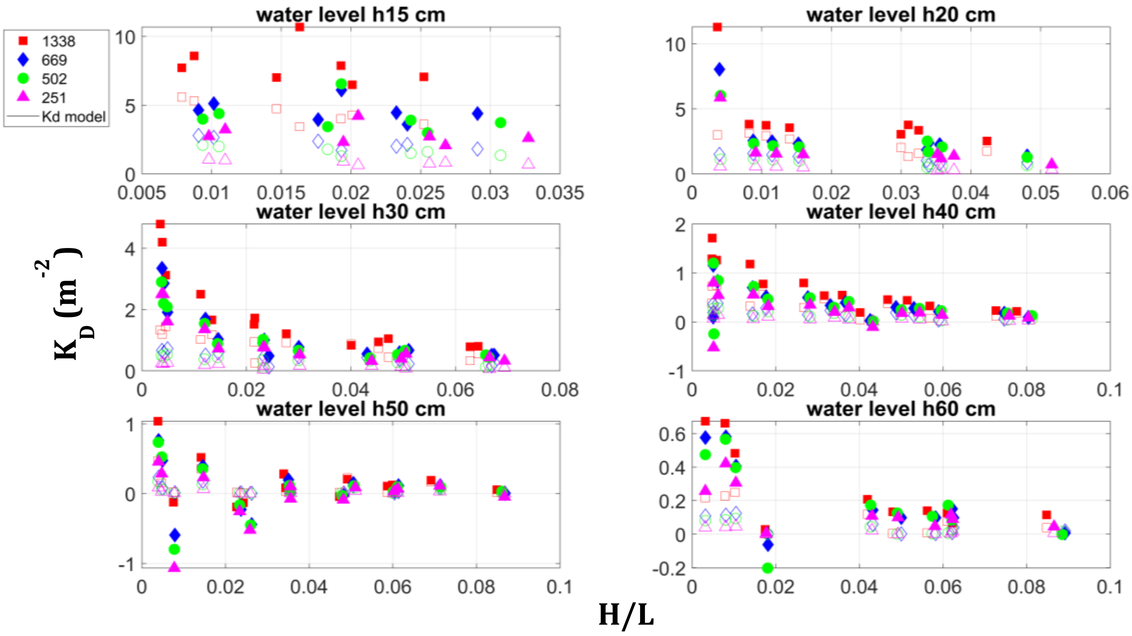

Fig 4.9 ***K_D*** **values variation with H/λ (at wg 7) for different water depths and seagrass densities**

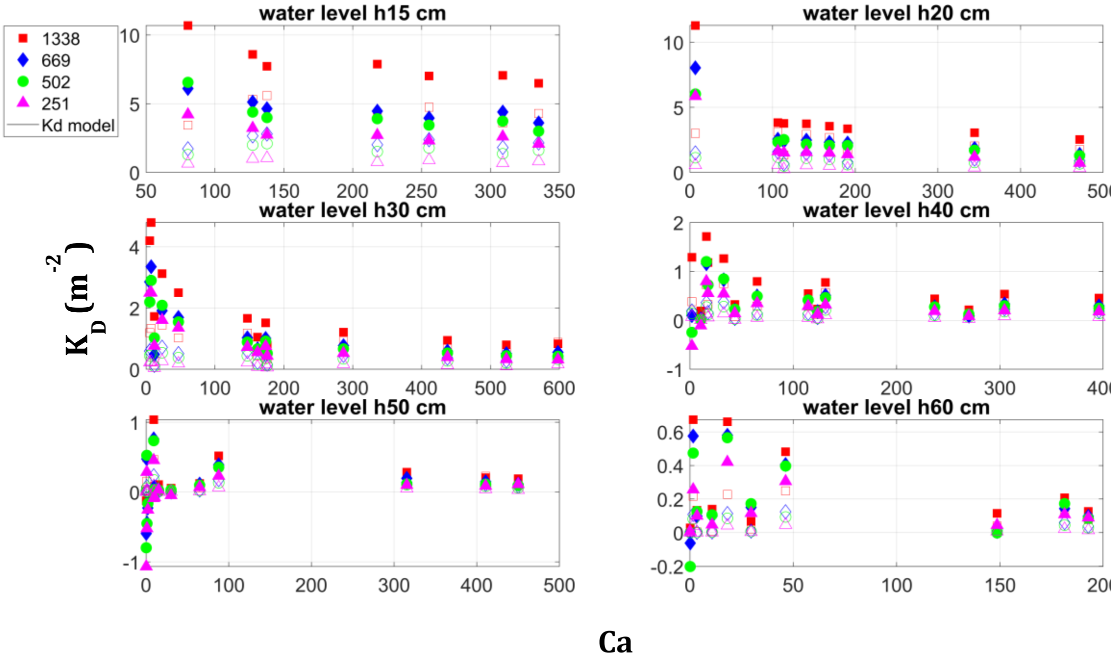

Fig 4.10 K_D values variation with Ca (at wg 7) for different water depths and seagrass densities

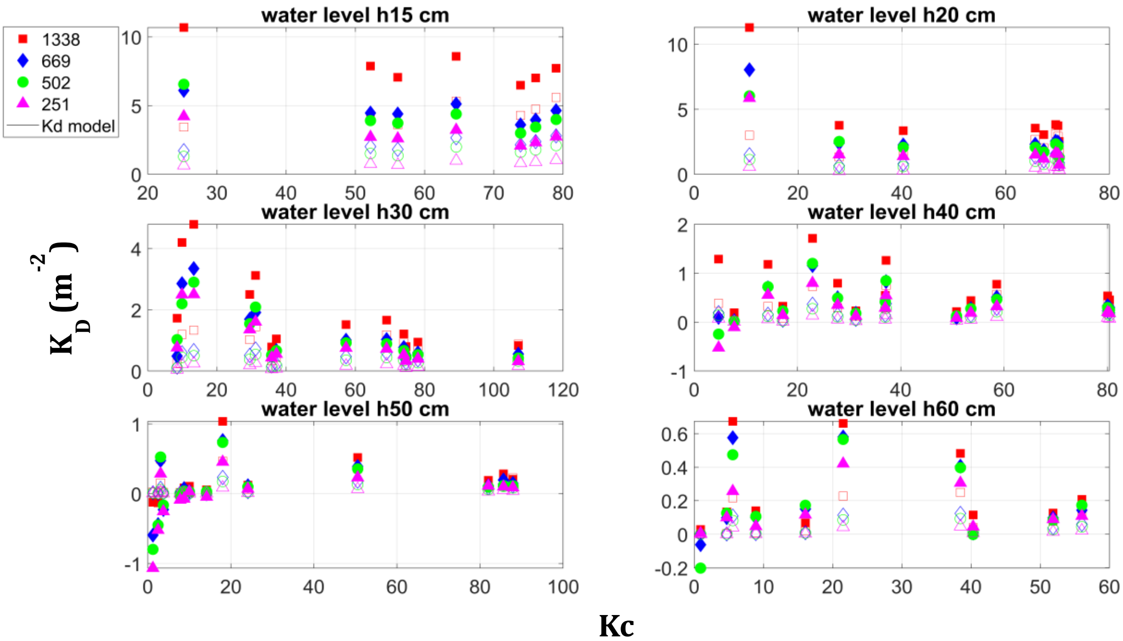

Fig 4.11 K_D values variation with Kc (at wg 7) for different water depths and seagrass densities

Chapter 5

Conclusions

Eelgrass meadow's potential in wave attenuation was assessed throughout a set of wave-vegetation interaction simulation experiments in a wave flume for a wide range of regular wave conditions and water depth and different plant densities. The linear wave theory was adopted for the data post-processing and analysis. The final goals were to evaluate to what extent waves are attenuated by eelgrass meadows and obtain a dissipation coefficient accordingly. Such a coefficient was then compared to an analytical model recently proposed in the literature that predicts the wave dissipation coefficient. Hence, the governing factors contributing to wave attenuation could be identified. As expected, the wave height decreases while passing over the meadows and this increases with the density of the plants. The estimated dissipation coefficients were in relatively good agreement with the predicted ones from the model in some cases. However, in a holistic framework, where for each water depth several experiments were conducted, not a promising alignment was observed between the model and experimental values of the dissipation coefficient.

Independent of all the other variables, wave height has an inverse relationship with the wave dissipation coefficient obtained in this study. Though it cannot be a key reason for the disagreement between our values and the models'. However, some other parameters such as water depth and wavelength may play a pivotal role. Dimensionless parameters such as the Cauchy number, the Keulegan-carpenter number, and the plant density turned out to be the most important factors affecting the dissipation coefficient value. In other words, when a wider range of these dimensionless parameters is involved (i.e., in the present study) compared to that leading to the analytical model, the resultant dissipation coefficients significantly differ from that of the proposed analytical model. This implies that the proposed model cannot yield a robust and rigorous result for the eelgrass wave dissipation coefficient.

Yet the contribution of other variables to the dissipation coefficient that was not addressed in this study has to be analysed in future efforts followed by field experiments to enhance the research quality. Hence, a more robust analytical model for the wave dissipation coefficient due to eelgrass meadows might be derived.

References

Airy, G. B. (1845). *Tides and waves*. B. Fellowes.

Asano, T., Deguchi, H., & Kobayashi, N. (1993). Interaction between water waves and vegetation. In *Proceedings of the Coastal Engineering Conference*. https://doi.org/10.1061/9780872629332.206

Balk, D., Montgomery, M., McGranahan, G., Kim, D., Mara, V., Todd, M., … Dorélien, A. (2009). Mapping urban settlements and the risks of climate change in Africa, Asia and South America. *Population Dynamics and Climate Change*.

Barbier, E. B. (2015). Climate change impacts on rural poverty in low-elevation coastal zones. *Estuarine, Coastal and Shelf Science*. https://doi.org/10.1016/j.ecss.2015.05.035

Benassai, G. (2006). *Introduction of Coastal Dynamics and Shoreline Protection*. *WIT Press*.

Borum, J., Duarte, C., Krause-Jensen, D., & Greve, T. M. (2004). European seagrasses : an introduction to monitoring and management. *Management*.

Bouma, T. J., De Vries, M. B., Low, E., Peralta, G., Tánczos, I. C., Van De Koppel, J., & Herman, P. M. J. (2005). Trade-offs related to ecosystem engineering: A case study on stiffness of emerging macrophytes. *Ecology*. https://doi.org/10.1890/04-1588

Bradley, K., & Houser, C. (2009). Relative velocity of seagrass blades: Implications for wave attenuation in low-energy environments. *Journal of Geophysical Research: Earth Surface*. https://doi.org/10.1029/2007JF000951

Charlier, R. H., Chaineux, M. C. P., & Morcos, S. (2005). Panorama of the history of coastal protection. *Journal of Coastal Research*. https://doi.org/10.2112/03561.1

Dalrymple, R. A., Kirby, J. T., & Hwang, P. A. (1984). Wave Diffraction Due to Areas of Energy Dissipation. *Journal of Waterway, Port, Coastal, and Ocean Engineering*. https://doi.org/10.1061/(asce)0733-950x(1984)110:1(67)

de los Santos, C. B., Vicencio-Rammsy, B., Lepoint, G., Remy, F., Bouma, T. J., & Gobert, S. (2016). Ontogenic variation and effect of collection procedure on leaf biomechanical properties of Mediterranean seagrass Posidonia oceanica (L.) Delile. *Marine Ecology*. https://doi.org/10.1111/maec.12340

Dean, R. G., & Dalrymple, R. A. (1984). Water wave mechanics for engineers and scientists. https://doi.org/10.1029/eo066i024p00490-06

Dugan, J. E., Airoldi, L., Chapman, M. G., Walker, S. J., & Schlacher, T. (2012). Estuarine and Coastal Structures: Environmental Effects, A Focus on Shore and Nearshore Structures. In *Treatise on Estuarine and Coastal Science*. https://doi.org/10.1016/B978-0-12-374711-2.00802-0

Dugan, Jenifer E., Hubbard, D. M., Rodil, I. F., Revell, D. L., & Schroeter, S. (2008). Ecological effects of coastal armoring on sandy beaches. *Marine Ecology*. https://doi.org/10.1111/j.1439-0485.2008.00231.x

Ferrario, F., Beck, M. W., Storlazzi, C. D., Micheli, F., Shepard, C. C., & Airoldi, L. (2014). The effectiveness of coral reefs for coastal hazard risk reduction and adaptation. *Nature Communications*. https://doi.org/10.1038/ncomms4794

Firth, L. B., Thompson, R. C., Bohn, K., Abbiati, M., Airoldi, L., Bouma, T. J., … Hawkins, S. J. (2014). Between a rock and a hard place: Environmental and engineering considerations when designing coastal defence structures. *Coastal Engineering*. https://doi.org/10.1016/j.coastaleng.2013.10.015

Galvin, C. J. (1964). *Wave-height prediction for wave generators in shallow water* (Vol. 4). Coastal Engineering Research Center.

Gerhart, D. J. (1990). Shore Ecology of the Gulf of Mexico . Joseph C. Britton , Brian Morton . *The Quarterly Review of Biology*. https://doi.org/10.1086/416780

Griggs, G., & Patsch, K. (2019). The Protection/Hardening of California's Coast: Times Are Changing. *Journal of Coastal Research*. https://doi.org/10.2112/JCOASTRES-D-19A-00007.1

Hemminga, M. A., & Duarte, C. M. (2000). *Seagrass Ecology*. *Seagrass Ecology*. https://doi.org/10.1017/cbo9780511525551

Hugo, G. (2011). Future demographic change and its interactions with migration and climate change. *Global Environmental Change*. https://doi.org/10.1016/j.gloenvcha.2011.09.008

Infantes, E., Orfila, A., Simarro, G., Terrados, J., Luhar, M., & Nepf, H. (2012). Effect of a seagrass (Posidonia oceanica) meadow on wave propagation. *Marine Ecology Progress Series*. https://doi.org/10.3354/meps09754

IPCC. (2022). Sea Level Rise and Implications for Low-Lying Islands, Coasts and Communities. In *The Ocean and Cryosphere in a Changing Climate*. https://doi.org/10.1017/9781009157964.012

Kaiser, G., & Witzki, D. (2004). Public perception of coastal flood defence and participation in coastal flood defence planning Results. *Coastline Reports*.

Kirwan, M. L., & Megonigal, J. P. (2013). Tidal wetland stability in the face of human impacts and sea-level rise. *Nature*. https://doi.org/10.1038/nature12856

Kirwan, M. L., Temmerman, S., Skeehan, E. E., Guntenspergen, G. R., & Fagherazzi, S. (2016). Overestimation of marsh vulnerability to sea level rise. *Nature Climate Change*. https://doi.org/10.1038/nclimate2909

Kobayashi, N., Raichle, A. W., & Asano, T. (1993). Wave Attenuation by Vegetation. *Journal of Waterway, Port, Coastal, and Ocean Engineering*. https://doi.org/10.1061/(asce)0733-950x(1993)119:1(30)

Lei, J., & Nepf, H. (2019). Wave damping by flexible vegetation: Connecting individual blade dynamics to the meadow scale. *Coastal Engineering*. https://doi.org/10.1016/j.coastaleng.2019.01.008

Lima, S. F., Neves, C. F., & Rosauro, N. M. L. (2007). DAMPING OF GRAVITY WAVES BY FIELDS OF FLEXIBLE VEGETATION. https://doi.org/10.1142/9789812709554_0043

Lucrezi, S., Schlacher, T. A., & Robinson, W. (2010). Can storms and shore armouring exert additive effectson sandy-beach habitats and biota? *Marine and Freshwater Research*. https://doi.org/10.1071/MF09259

Luhar, M., Infantes, E., & Nepf, H. (2017). Seagrass blade motion under waves and its impact on wave decay. *Journal of Geophysical Research: Oceans*. https://doi.org/10.1002/2017JC012731

Luhar, M., & Nepf, H. M. (2016). Wave-induced dynamics of flexible blades. *Journal of Fluids and Structures*. https://doi.org/10.1016/j.jfluidstructs.2015.11.007

Manca, E., Cáceres, I., Alsina, J. M., Stratigaki, V., Townend, I., & Amos, C. L. (2012). Wave energy and wave-induced flow reduction by full-scale model Posidonia oceanica seagrass. *Continental Shelf Research*. https://doi.org/10.1016/j.csr.2012.10.008

Mangan, J., Lalwani, C., & Fynes, B. (2008). Port-centric logistics. *The International Journal of Logistics Management*. https://doi.org/10.1108/09574090810872587

McGranahan, G., Balk, D., & Anderson, B. (2007). The rising tide: Assessing the risks of climate change and human settlements in low elevation coastal zones. *Environment and Urbanization*. https://doi.org/10.1177/0956247807076960

Mendez, F. J., & Losada, I. J. (2004). An empirical model to estimate the propagation of random breaking and nonbreaking waves over vegetation fields. *Coastal Engineering*. https://doi.org/10.1016/j.coastaleng.2003.11.003

Méndez, F. J., Losada, I. J., & Losada, M. A. (1999). Hydrodynamics induced by wind waves in a vegetation field. *Journal of Geophysical Research: Oceans*. https://doi.org/10.1029/1999jc900119

Neumann, B., Vafeidis, A. T., Zimmermann, J., & Nicholls, R. J. (2015). Future coastal population growth and exposure to sea-level rise and coastal flooding - A global assessment. *PLoS ONE*. https://doi.org/10.1371/journal.pone.0118571

Nordstrom, K. F. (2014). Living with shore protection structures: A review. *Estuarine, Coastal and Shelf Science*. https://doi.org/10.1016/j.ecss.2013.11.003

Ondiviela, B., Losada, I. J., Lara, J. L., Maza, M., Galván, C., Bouma, T. J., & van Belzen, J. (2014). The role of seagrasses in coastal protection in a changing climate. *Coastal Engineering*. https://doi.org/10.1016/j.coastaleng.2013.11.005

OTA, T., KOBAYASHI, N., & KIRBY, J. T. (2005). WAVE AND CURRENT INTERACTIONS WITH VEGETATION. https://doi.org/10.1142/9789812701916_0040

Pilarczyk, K. W. (2003). Design of low-crested (submerged) structures – an overview –. *6th Intern. Conf. on Coastal and Port Engineering in Developing Countries*.

Pontee, N., Narayan, S., Beck, M. W., & Hosking, A. H. (2016). Nature-based solutions: Lessons from around the world. *Proceedings of the Institution of Civil Engineers: Maritime Engineering*. https://doi.org/10.1680/jmaen.15.00027

Radder, A. C. (1979). On the parabolic equation method for water-wave propagation. *Journal of Fluid Mechanics*. https://doi.org/10.1017/S0022112079001397

Reguero, B. G., Losada, I. J., & Méndez, F. J. (2019). A recent increase in global wave power as a consequence of oceanic warming. *Nature Communications*. https://doi.org/10.1038/s41467-018-08066-0

Repolho, T., Duarte, B., Dionísio, G., Paula, J. R., Lopes, A. R., Rosa, I. C., … Rosa, R. (2017). Seagrass ecophysiological performance under ocean warming and acidification. *Scientific Reports*. https://doi.org/10.1038/srep41443

Schoonees, T., Gijón Mancheño, A., Scheres, B., Bouma, T. J., Silva, R., Schlurmann, T., & Schüttrumpf, H. (2019). Hard Structures for Coastal Protection, Towards Greener Designs. *Estuaries and Coasts*. https://doi.org/10.1007/s12237-019-00551-z

Seto, K. C., Fragkias, M., Güneralp, B., & Reilly, M. K. (2011). A meta-analysis of global urban land expansion. *PLoS ONE*. https://doi.org/10.1371/journal.pone.0023777

Stratigaki, V., Manca, E., Prinos, P., Losada, I. J., Lara, J. L., Sclavo, M., … Sánchez-Arcilla, A. (2011). Large-scale experiments on wave propagation over Posidonia oceanica. *Journal of Hydraulic Research*. https://doi.org/10.1080/00221686.2011.583388

U S Army Corps Of Engineers, N. (2002). Coastal Engineering Manual. *Coastal Engineering Manual*.

Zhao, R., Hynes, S., & Shun He, G. (2014). Defining and quantifying China's ocean economy. *Marine Policy*. https://doi.org/10.1016/j.marpol.2013.05.008

Appendix

Table A.1 wave conditions used for the experiments

h (m)	freq & height	exp 1	exp 2	exp 3	exp 4	exp 5	exp 6	exp 7	exp 8	exp 9	exp 10	exp 11	exp 12	exp 13	exp 14
0.15	f (Hz)	0.457	0.535	1.072	0.646	0.863	0.761	0.957							
	H (m)	0.031	0.030	0.026	0.043	0.042	0.052	0.050							
0.2	f (Hz)	0.723	0.454	0.519	0.605	1.152	1.041	0.844	0.947						
	H (m)	0.008	0.032	0.037	0.041	0.041	0.051	0.065	0.078						
0.3	f (Hz)	0.610	0.468	1.221	0.538	0.702	1.037	1.122	0.823	0.941	0.702	0.702	0.702	0.702	
	H (m)	0.011	0.018	0.024	0.048	0.056	0.070	0.081	0.097	0.116	0.010	0.029	0.074	0.106	
0.4	f (Hz)	0.876	0.524	0.466	1.241	0.597	1.151	0.670	1.073	0.761	0.985	0.876	0.876	0.876	0.876
	H (m)	0.009	0.019	0.026	0.042	0.056	0.068	0.093	0.100	0.118	0.125	0.027	0.053	0.070	0.102
0.5	f (Hz)	0.903	0.506	1.247	1.087	0.565	1.160	1.005	0.637	0.709	0.795	1.160	1.160	1.160	1.160
	H (m)	0.009	0.016	0.026	0.046	0.053	0.070	0.091	0.113	0.140	0.162	0.009	0.027	0.054	0.100
0.6	f (Hz)	0.669	1.249	0.594	0.536	1.164	1.093	1.014	0.733	0.815	0.917				
	H (m)	0.0093	0.01785238	0.0291	0.0431	0.0555	0.0742	0.0933	0.114	0.1383	0.1565				